Advective Diffusion of Contaminants in the Surf Zone

Patricio Winckler[1]; Philip L.-F. Liu, Dist.M.ASCE[2]; and Chiang C. Mei[3]

Abstract: A theory on the horizontal spreading of contaminants in the surf zone is described in this paper. The surf zone is viewed as a narrow strip comparable to the characteristic wavelength, in which turbulence caused by wave breaking is strong. Flows inside the surf zone consist of both oscillatory motions and a steady current induced by breaking waves. The wave field in the shoaling zone is modeled by the linear theory for monochromatic waves, and it is assumed that the breaking wave height is proportional to the local depth in the surf zone. The simplest scenario of longshore current on a straight beach of constant slope is considered, for which the longshore current velocity is predicted by a slightly modified version of Longuet-Higgins' original theory developed in the 1970s. On the basis of the estimation that the time scale of horizontal diffusion is much longer than the wave period, the perturbation method of multiple scales is applied to derive the transport equation for the advective diffusion of a solute. The total advection velocity is found to be the sum of the steady current caused by radiation stresses and a contribution from the covariance of fluctuating velocity and concentration, which is the same as the Stokes drift in periodic waves. Numerical predictions for the movement of a solute cloud released, instantaneously or continuously, in a longshore current along a plane beach are examined. The solute is found to drift shoreward in addition to the expected transport along the shore. Computed examples are presented and comparisons with available laboratory experiments are also discussed. **DOI: 10.1061/(ASCE)WW.1943-5460.0000196.**

CE Database subject headings: Solutes; Advection; Surf zones; Water pollution; Pollutants; Littoral currents.

Author keywords: Solute transport; Advection; Diffusion; Wave breaking; Surf zone; Longshore current; Multiple scales perturbation method.

Introduction

In engineering practice, mixing of contaminants in the ocean is usually assessed by means of depth-averaged transport models that require knowledge of the flow field and empirical coefficients to predict concentrations within a particular site. Several theories have been proposed to predict the mixing and transport of contaminants in shallow waters. Fischer et al. (1979) proposed a two-dimensional (2D) depth-integrated transport equation averaged over a tidal cycle to assess mixing processes in estuaries, whereas Rutherford (1994) derived a similar equation to evaluate mixing in rivers where shear dispersion caused by vertical variations of the velocity is dominant. For solute transport in the surf zone, Harris et al. (1963) and Inman et al. (1971) took the first steps by estimating the magnitude of turbulent diffusivity from field data based on the simple diffusion equation.

In recent years, there have been extensive field measurements on natural beaches. For example, Takewaka et al. (2003) reported video images taken at PARI's Oceanographical Research Station located in Hasaki, Japan, on the evolution of a dye patch released outside the main surf zone. Unfortunately the current measurements were only taken outside the main surf zone, and the dye patch never entered the breakers. Spydell et al. (2007, 2009) reported observations of drifter movement on a natural beach and suggested a mathematical model where the diffusivity is expressed as a convolution integral. Clarke et al. (2007) described field observations of dye transport on a natural beach where rip currents were also present and used a simple advection-diffusion model to simulate shoreline concentration time series for an idealized surf zone. Feddersen (2007) proposed a model by assuming that the mass itself is diffused like heat and convected by the longshore velocity. Laboratory experiments have also been conducted using simple geometries. Sun and Tao (2003) carried out experiments on a straight and plane beach in a rectangular wave basin and described a numerical model based on the mild-slope equation for waves and the full advective diffusion equation for the solute transport. Pearson et al. (2009) examined the mixing process for normally incident waves combined with an externally imposed longshore current in the laboratory experiments to estimate the cross-shore mixing coefficients.

For a better understanding of the physics behind the transport process in the surf zone, more analytical work will be useful to help ascertain the detailed role of incident waves. Although future mathematical models must be highly numerical to account for a multitude of complex factors in nature such as coastal geography, nonlinearity in wave climate, rip currents, wind, and tides, etc., approximate theories and rigorously controlled experiments for simple systems can sharpen the understanding of the role of each factor. An essentially analytical theory for dye release near and inside the surf zone along a plane beach, caused by breaking of a monochromatic wave train, is reported herein. The classical theory of longshore currents by Longuet-Higgins (1970a, b) is adopted to calculate longshore current velocity using wave amplitudes according to the linear theory for monochromatic waves in both the shoaling and surf zones. Assuming the solute to be vertically well mixed, an

[1]Associate Professor, Escuela de Ingenieria Civil Oceanica, Univ. de Valparaiso, Valparaiso 33449, Chile; and Graduate Student, School of Civil and Environmental Engineering, Cornell Univ., Ithaca, NY 14853 (corresponding author). E-mail: paw87@cornell.edu

[2]Class of 1912 Professor, School of Civil and Environmental Engineering, Cornell Univ., Ithaca, NY 14853; and Kwoh-Ting Li Chair Professor, Institute of Hydrological and Oceanic Sciences, National Central University, Jhongli, Taiwan.

[3]Ford Professor Emeritus, Dept. of Civil and Environmental Engineering, Massachusetts Institute of Technology, Cambridge, MA 02139.

Note. This manuscript was submitted on September 8, 2012; approved on January 15, 2013; published online on January 17, 2013. Discussion period open until April 1, 2014; separate discussions must be submitted for individual papers. This paper is part of the ***Journal of Waterway, Port, Coastal, and Ocean Engineering***, Vol. 139, No. 6, November 1, 2013. ©ASCE, ISSN 0733-950X/2013/6-437–454/$25.00.

advective-diffusion equation for the slow time transport of solute in the horizontal plane is derived. Using multiple-scale analysis, it is shown that in addition to longshore current, Stokes drift is also responsible for solute transport inside and outside of the surf zone. Numerical examples are presented for a variety of wave conditions to model the transport of a dye cloud released inside or slightly outside the surf zone. Comparisons with available laboratory and field experiments are discussed.

Theoretical Background

The solute concentration in shallow water is assumed to be constant in depth because of either effective vertical mixing or negligible buoyancy. Conservation of solute in a vertical column of water is

$$\frac{\partial\left[(\eta'+\overline{h})C\right]}{\partial t}+\frac{\partial\left[u(\eta'+\overline{h})C\right]}{\partial x}+\frac{\partial\left[v(\eta'+\overline{h})C\right]}{\partial y}=\frac{\partial}{\partial x}\left[(\eta'+\overline{h})K_x\frac{\partial C}{\partial x}\right]+\frac{\partial}{\partial y}\left[(\eta'+\overline{h})K_y\frac{\partial C}{\partial y}\right]+q \quad (1)$$

where $C(x,y,t)$ = depth-averaged concentration; $\eta'(x,y,t)$ = fluctuating part of the free surface elevation; $\overline{h}(x,y)$ = time-averaged water depth over a period accounting for set-down and setup as detailed in the section Mean Free Surface; $u(x,y,t)$ and $v(x,y,t)$ = cross-shore and longshore velocities, respectively; and K_x and K_y = cross-shore and longshore turbulent diffusivities, respectively. Finally, $q(x,y,t)$ = rate of solute discharge per unit area.

Assuming small wave amplitudes, $\eta' \ll \overline{h}$, the transport equation can be linearized to

$$\frac{\partial C}{\partial t}+u\frac{\partial C}{\partial x}+v\frac{\partial C}{\partial y}=\frac{1}{\overline{h}}\left[\frac{\partial}{\partial x}\left(\overline{h}K_x\frac{\partial C}{\partial x}\right)+\frac{\partial}{\partial y}\left(\overline{h}K_y\frac{\partial C}{\partial y}\right)\right]+\frac{q}{\overline{h}} \quad (2)$$

after invoking conservation of water mass

$$\frac{\partial \eta'}{\partial t}+\frac{\partial(u\overline{h})}{\partial x}+\frac{\partial(v\overline{h})}{\partial y}=0 \quad (3)$$

This linearization is also the basis of the existing longshore current theory (Longuet-Higgins 1970a, b), which is justifiable only in the shoaling zone but not in the surf zone. Because this simplification has nevertheless proven to be successful in predicting longshore current, it is adopted here despite its crudeness.

Order Estimates

The wave period $T=2\pi/\omega$ is chosen to characterize time and the wavelength $\lambda_0=2\pi/k_0$ to characterize horizontal distances including the surf zone width, where ω is the frequency of the incident wave and $k_0=\omega/\sqrt{gh_0}$ is the wave number at the depth h_0. Introducing the following normalizations

$$(x',y')=\frac{(x,y)}{\lambda_0},\quad t'=\frac{t}{T},\quad (u',v')=\frac{Th_0}{\lambda_0 A_0}(u,v),\quad \overline{h}'=\frac{\overline{h}}{h_0},$$
$$(K_x',K_y')=\frac{(K_x,K_y)}{K_b},\quad C'=\frac{C}{C_0},\quad \frac{q'}{\overline{h}'}=\frac{q}{\overline{h}}\frac{T_s}{C_0} \quad (4)$$

where A_0, K_b, and C_0 = characteristic wave amplitude, turbulent diffusivity, and concentration, respectively, and T_s = time scale of solute release, assumed to be much longer than the wave period. Substituting these dimensionless variables into Eq. (2)

$$\frac{\partial C'}{\partial t'}+\frac{A_0}{h_0}\left(u'\frac{\partial C'}{\partial x'}+v'\frac{\partial C'}{\partial y'}\right)=\frac{TK_b}{\lambda_0^2}\frac{1}{\overline{h}'}\left[\frac{\partial}{\partial x'}\left(\overline{h}'K_x'\frac{\partial C'}{\partial x'}\right)+\frac{\partial}{\partial y'}\left(\overline{h}'K_y'\frac{\partial C'}{\partial y'}\right)\right]+\frac{T}{T_s}\frac{q'}{\overline{h}'} \quad (5)$$

in which A_0/h_0 = nonlinearity of wave motion; TK_b/λ_0^2 = ratio of wave period to diffusion time; and T/T_s = ratio of wave period to solute release time. Inman et al. (1971) suggested a cross-shore diffusivity given by $K_b=\mathcal{O}(2A_bx_b/T)$, where A_b = root mean square breaker amplitude; x_b = width of the surf zone; and T = peak period of the wave energy spectra. As an example, let $2A_b=1\,\mathrm{m}$, $x_b=10\,\mathrm{m}$, and $T=10\,\mathrm{s}$, then $K_b=\mathcal{O}(1)\mathrm{m}^2/\mathrm{s}$. Comparable estimates from field observations have been reported by Takewaka et al. (2003), Mariani (2004), Clark et al. (2010), and others. In addition to weak nonlinearity

$$\frac{A_0}{h_0}=\varepsilon\ll 1 \quad (6)$$

also assumed is

$$\frac{TK_b}{\lambda_0^2}=O\left(\varepsilon^2\right),\quad \frac{T}{T_s}=O\left(\varepsilon^2\right) \quad (7)$$

so that advection, diffusion, and mass supply will be of comparable importance after many wave periods. Returning to physical variables but retaining ϵ as the ordering parameter, the solute transport [Eq. (5)] is rewritten as follows:

$$\frac{\partial C}{\partial t}+\varepsilon\left(u\frac{\partial C}{\partial x}+v\frac{\partial C}{\partial y}\right)=\frac{\varepsilon^2}{\overline{h}}\left[\frac{\partial}{\partial x}\left(\overline{h}K_x\frac{\partial C}{\partial x}\right)+\frac{\partial}{\partial y}\left(\overline{h}K_y\frac{\partial C}{\partial y}\right)\right]+\varepsilon^2\frac{q(x,y,\varepsilon^2 t)}{\overline{h}} \quad (8)$$

The order contrast among terms in this equation is similar to that for the dispersion of suspended sediments in a wave-induced boundary layer near the seabed (Mei and Chian 1994; Mei et al. 1997, 1998). Because of the sharp difference between the time scales of wave oscillations and diffusion, the perturbation method of multiple scales (i.e., homogenization) can be used.

Equation for Long-Time Transport

Limiting to monochromatic waves of small amplitudes, the velocity components in the following perturbation series are expanded:

$$u=u_0(x,y,t)+\varepsilon u_1(x,y,t)+\varepsilon^2u_2(x,y,t)+\cdots$$
$$v=v_0(x,y,t)+\varepsilon v_1(x,y,t)+\varepsilon^2v_2(x,y,t)+\cdots \quad (9)$$

where

$$u_0=\mathrm{Re}\left(U_0e^{-i\omega t}\right),\quad v_0=\mathrm{Re}\left(V_0e^{-i\omega t}\right) \quad (10)$$

and $\mathrm{Re}(\cdot)$ denotes the real part of $(\cdot)$. Note that (u_1, v_1) consists of zeroth and second harmonics, etc. Unlike the waves, solute concentration varies according to two contrasting time scales. Hence, the fast time $t=\mathcal{O}(2\pi/\omega)$ is introduced for the wave motion, and the slow time $\tau=\varepsilon^2t=O(\lambda_0^2/K_b)$ for the effects of diffusion. Thus, the concentration $C(x,y,t,\tau)$ depends on (t,τ) as independent

J. Waterway, Port, Coastal, Ocean Eng. 2013.139:437-454.

variables so that the original time derivative is replaced by $\partial C/\partial t + \epsilon^2 \partial C/\partial \tau$. By averaging over the wave period (i.e., the fast time), the slow evolution of the mean concentration can be found. From Eq. (8) it is evident that C is independent of the fast time t at the leading order; hence, the following two-scale expansion is assumed:

$$C = C_0(x, y, \tau) + \varepsilon C_1(x, y, t, \tau) + \varepsilon^2 C_2(x, y, t, \tau) + \cdots \tag{11}$$

Introducing Eqs. (9) and (11) in Eq. (8) yields a sequence of perturbation equations for solute transport at different orders. The order $\mathcal{O}(1)$ equation is trivially satisfied by the period-average C_0. At $\mathcal{O}(\epsilon)$

$$\frac{\partial C_1}{\partial t} + u_0 \frac{\partial C_0}{\partial x} + v_0 \frac{\partial C_0}{\partial y} = 0 \tag{12}$$

Because u_0 and v_0 are simple harmonic in t, so is C_1

$$C_1 = -\frac{1}{\omega} \mathrm{Re}\left[i \left(U_0 \frac{\partial C_0}{\partial x} + V_0 \frac{\partial C_0}{\partial y} \right) e^{-i\omega t} \right] \tag{13}$$

Thus, C_1 oscillates periodically with frequency, ω, with a slowly varying amplitude, which is to be determined. At $\mathcal{O}(\epsilon^2)$, the perturbation equation is

$$\begin{aligned} &\frac{\partial C_0}{\partial \tau} + \frac{\partial C_2}{\partial t} + u_0 \frac{\partial C_1}{\partial x} + u_1 \frac{\partial C_0}{\partial x} + v_0 \frac{\partial C_1}{\partial y} + v_1 \frac{\partial C_0}{\partial y} \\ &\quad = \frac{1}{\overline{h}} \frac{\partial}{\partial x} \left(\overline{h} K_x \frac{\partial C_0}{\partial x} \right) + \frac{1}{\overline{h}} \frac{\partial}{\partial y} \left(\overline{h} K_y \frac{\partial C_0}{\partial y} \right) + \frac{q(x, y, \tau)}{\overline{h}} \end{aligned} \tag{14}$$

Its time average over a wave period is

$$\begin{aligned} &\frac{\partial C_0}{\partial \tau} + \frac{\partial \overline{C_2}}{\partial t} + \overline{u_0 \frac{\partial C_1}{\partial x}} + \overline{v_0 \frac{\partial C_1}{\partial y}} + \overline{u_1} \frac{\partial C_0}{\partial x} + \overline{v_1} \frac{\partial C_0}{\partial y} \\ &\quad = \frac{1}{\overline{h}} \frac{\partial}{\partial x} \left(\overline{h} K_x \frac{\partial C_0}{\partial x} \right) + \frac{1}{\overline{h}} \frac{\partial}{\partial y} \left(\overline{h} K_y \frac{\partial C_0}{\partial y} \right) + \frac{q(x, y, \tau)}{\overline{h}} \end{aligned} \tag{15}$$

where the time average over a wave period is defined as

$$\overline{f} = \frac{\omega}{2\pi} \int_{t_0}^{t_0 + T} f(\xi)\, d\xi \tag{16}$$

In Eq. (15), $\partial \overline{C_2}/\partial t = 0$, because the time-averaged quantity is independent of fast time, t. Substituting Eq. (13) into Eq. (15) and using the well-known properties of products of sinusoidal functions

$$\begin{aligned} &\frac{\partial C_0}{\partial \tau} + \left[\overline{u}_1 + \frac{1}{2\omega} \mathrm{Re}\left(i U_0 \frac{\partial U_0^*}{\partial x} + i V_0 \frac{\partial U_0^*}{\partial y} \right) \right] \frac{\partial C_0}{\partial x} \\ &\quad + \left[\overline{v}_1 + \frac{1}{2\omega} \mathrm{Re}\left(i U_0 \frac{\partial V_0^*}{\partial x} + i V_0 \frac{\partial V_0^*}{\partial y} \right) \right] \frac{\partial C_0}{\partial y} \\ &\quad = \frac{1}{\overline{h}} \frac{\partial}{\partial x} \left(\overline{h} K_x \frac{\partial C_0}{\partial x} \right) + \frac{1}{\overline{h}} \frac{\partial}{\partial y} \left(\overline{h} K_y \frac{\partial C_0}{\partial y} \right) + \frac{q(x, y, \tau)}{\overline{h}} \end{aligned} \tag{17}$$

This result is similar to that governing the dispersion of suspended sediment in a wave boundary layer by Mei and Chian (1994) and Mei et al. (1997, 1998). The advective velocity consists of two parts. The components $\overline{u}_1$ and $\overline{v}_1$ represent the near-shore circulation induced by breaking waves. The quadratic terms inside the brackets arise from cross-correlations between fluctuations of flow and concentration, which would not exist without the solute. These velocity components are identical to the Stokes drift for monochromatic waves (Mei et al. 2005, p. 516)

$$\overline{\left[\int^t \mathbf{u}_0\, dt' \right] \cdot \nabla \mathbf{u}_0(\mathbf{x}, t)} \tag{18}$$

where ∇ = 2D horizontal gradient vector; and $\mathbf{u}_0$ = wave velocity vector, whose components are given in Eq. (10). Thus, the total advective velocity responsible for transporting the solute is the sum of the Eulerian mean current generated by breaking waves, $(\overline{u}_1, \overline{v}_1)$, and the Stokes drift and can be viewed as the mass transport velocity (Hunt and Johns 1963).

In later examples, two types of pollutant release will be considered: (1) continuous release and (2) instantaneous release. For continuous release, the source term $q(x, y, \tau)$ in Eq. (17) is modeled by

$$q(x, y, \tau) = \tilde{Q}(x, y) H(\tau) \tag{19}$$

where $H(\tau)$ = Heaviside step function; and $\tilde{Q}(x, y)$ = rate of discharge per unit area. For instantaneous release, the initial value problem governed by the homogeneous version of Eq. (17) subjected to the initial condition

$$C(x, y, 0+) = \tilde{C}(x, y) \tag{20}$$

is solved.

This is equivalent to the source function

$$q(x, y, \tau) = \overline{h} \tilde{C}(x, y) \delta(\tau) \tag{21}$$

where $\delta(\tau)$ is the delta function.

In subsequent examples, sources of continuous [Eq. (19)] and instantaneous [Eq. (21)] release are modeled, respectively, by the 2D Gaussian function defined as follows:

$$\left\{ \begin{matrix} \tilde{Q}(x, y) \\ \tilde{C}(x, y) \end{matrix} \right\} = \left\{ \begin{matrix} \tilde{Q}_{\max} \\ \tilde{C}_{\max} \end{matrix} \right\} \exp\left[-\frac{(x - x_0)^2}{2\sigma_x^2} - \frac{(y - y_0)^2}{2\sigma_y^2} \right] \tag{22}$$

in which $\tilde{Q}_{\max}$ and $\tilde{C}_{\max}$ = maximum values of the rate of discharge per unit area and concentration at (x_0, y_0) for the continuous and instantaneous sources, respectively. $\tilde{C}_{\max}$ can be either dimensionless (e.g., volume of solute/volume of solvent) or dimensional (e.g., mass of solute/volume of solvent). Here a dimensionless concentration $\tilde{C}_{\max}$ is used, and thus $\tilde{Q}_{\max}$ has units of ms^{-1}.

Transport along a Straight Coast

Consider a straight beach with static depth $h(x)$ where the coordinate x is orthogonal to the shoreline (Fig. 1). The still-water shoreline is located at $x = 0$. A train of monochromatic waves with frequency ω and amplitude A propagates from deep water toward the coast with a local angle of incidence θ. In the shoaling zone outside the breaker line, $x > x_b$, the free surface elevation can be given by the ray approximation for small amplitude waves. Accordingly, the local wave direction $\theta(x)$ obeys Snell's law

$$\beta = k \sin\theta = \beta_0 = k_0 \sin\theta_0 \tag{23}$$

which implies

$$\alpha = k \cos\theta = \sqrt{k^2 - \beta^2} \tag{24}$$

J. Waterway, Port, Coastal, Ocean Eng. 2013.139:437-454.

In very shallow water, the local wave number $k(x)$ is related to the local depth $h(x)$ by the approximate dispersion relation

$$\omega = k\sqrt{gh} \tag{25}$$

Let the local free surface displacement be

$$\eta = \mathrm{Re}\left[Ae^{-i\left(\int \alpha dx - \beta y + \omega t\right)}\right] \tag{26}$$

Near the shore where water is shallow, it is assumed that Eqs. (23)–(26) still hold even inside the surf zone, but can be further approximated for $kh \ll 1$ so that

$$(u_0, v_0) \sim \mathrm{Re}\left[(U_0, V_0)e^{-i\omega t}\right] = (\alpha, \beta)\mathrm{Re}\left[\frac{gA}{\omega}e^{-i\left(\int \alpha dx - \beta y + \omega t\right)}\right] \tag{27}$$

Outside the breaker line, the wave amplitude A can be approximated by Green's law

$$\frac{A(x)}{A_0} = \sqrt{\frac{C_{g0}}{\sqrt{gh}}\frac{\cos\theta_0}{\cos\theta}}, \quad x > x_b \tag{28}$$

In the surf zone, the common assumption that the breaking-wave amplitude decreases with local depth is adopted (Munk 1949)

$$A(x) = \gamma\overline{h}(x)/2, \quad -x_s < x < x_b \tag{29}$$

The empirical value of the breaker coefficient varies in the range $\gamma = 0.73-1.03$ (Svendsen 2006) depending on the type of breakers.

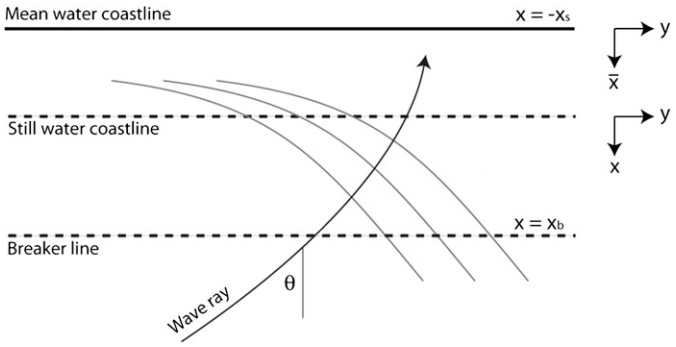

Fig. 1. Monochromatic waves approaching a straight shoreline at an oblique angle

Longuet-Higgins (1970a) proposed values between $\gamma = 0.6$ and 1.2 from a series of studies based on direct observations and laboratory measurements.

Mean Free Surface

Longuet-Higgins (1964) found that in shallow waters outside the breaker line, the mean free surface is lower than the still water level by the set-down

$$\overline{\eta} = -\frac{A^2}{4h}, \quad x > x_b \tag{30}$$

Thus, the mean total water depth outside the breaker line is

$$\overline{h} = \overline{\eta} + h = \left[1 - \frac{1}{4}\left(\frac{A}{h}\right)^2\right]h, \quad x > x_b \tag{31}$$

and at the breaker line

$$\overline{h}_b = \overline{\eta}_b + h_b = \left(1 - \frac{\gamma^2}{16}\right)h_b \tag{32}$$

which differs little from h_b. Inside the surf zone, there is a setup of the mean free surface as a consequence of the radiation stress (Longuet-Higgins 1970b)

$$\overline{h} = \frac{1}{1 + \frac{3}{8}\gamma^2}(h - h_s) \tag{33}$$

where

$$h_s = -\left(\overline{\eta}_b + \frac{3}{8}\gamma^2\overline{h}_b\right) = -\frac{5\gamma^2}{16}h_b \tag{34}$$

The location of the mean shoreline is determined from $\overline{h} = 0$, i.e.,

$$x_s = -\frac{5\gamma^2}{16}x_b \tag{35}$$

It is convenient to adopt a new coordinate

$$\overline{x} = x - x_s \tag{36}$$

so that the surf zone is defined as $0 < \overline{x} < \overline{x}_b$ (Figs. 1 and 2). For the special case of a plane beach, $h = sx$, the mean total depth becomes

$$\overline{h} = \overline{\eta} + h = \overline{sx} \tag{37}$$

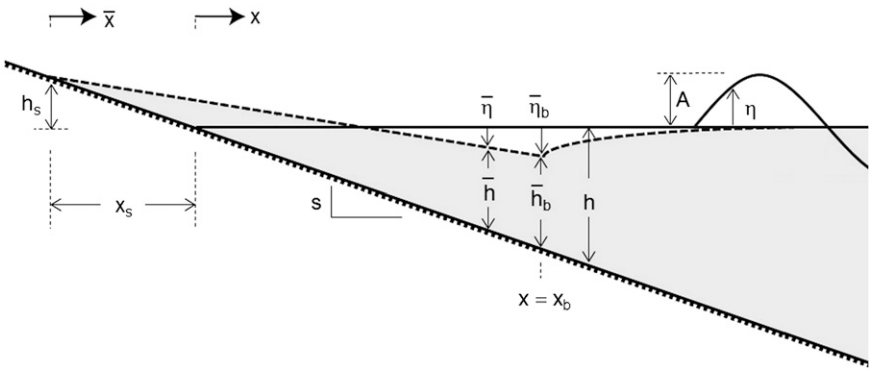

Fig. 2. Definition of parameters used for the wave set-down and setup

J. Waterway, Port, Coastal, Ocean Eng. 2013.139:437-454.

where

$$\overline{s} = \frac{s}{1 + \frac{3}{8}\gamma^2} \tag{38}$$

Longshore Current

The classic theory by Longuet-Higgins (1970a, b) is based on the following equations of mean momentum balance in the longshore direction

$$\begin{aligned} &\tau_y + \frac{\partial}{\partial \overline{x}}\left(\rho \nu \overline{h}\,\frac{\partial \overline{v}_1}{\partial \overline{x}}\right) - \langle B_y \rangle = 0, \quad 0 < \overline{x} < \overline{x}_b \\ &\frac{\partial}{\partial \overline{x}}\left(\rho \nu \overline{h}\,\frac{\partial \overline{v}_1}{\partial \overline{x}}\right) - \langle B_y \rangle = 0, \quad \overline{x}_b < \overline{x} < \infty \end{aligned} \tag{39}$$

where τ_y = radiation stress, which vanishes in the shoaling zone without breaking. Again, these equations are the second-order consequences based on linearization.

The period-averaged bottom friction is assumed to be proportional to the longshore current

$$\langle B_y \rangle = \frac{1}{\pi}\gamma C_f \rho \left(g\overline{h}\right)^{1/2} \overline{v}_1 = \left(\frac{1}{\pi}\gamma C_f \rho g^{1/2}\,\overline{s}^{1/2}\right)\overline{x}^{1/2}\overline{v}_1, \quad 0 < \overline{x} < \infty \tag{40}$$

where C_f = bottom friction coefficient; and ρ = density of water. By invoking the empirical relation [Eq. (29)], the radiation stress inside and outside of the surf zone is taken to be

$$\begin{aligned} \tau_y &= \frac{5}{16}\gamma^2 \rho \left(g\overline{h}\right)^{3/2} \frac{\sin\theta_b}{c_b}\frac{d\overline{h}}{d\overline{x}} \\ &= \left(\frac{5}{16}\gamma^2 \rho g \overline{s}^{5/2} \sin\theta_b \overline{h}_b^{-1/2}\right)\overline{x}^{3/2}, \quad 0 < \overline{x} < \overline{x}_b, \\ \tau_y &= 0, \quad \overline{x}_b < \overline{x} < \infty \end{aligned} \tag{41}$$

where θ_b and c_b = local angle of incidence and the local wave celerity at the breaker line, respectively.

To find an analytical solution for the longshore current from Eq. (39), Longuet-Higgins (1970b) assumed an eddy viscosity, ν, to be proportional to the distance from the mean shoreline

$$\nu = N\overline{x}\left(g\overline{h}\right)^{1/2} = N g^{1/2}\,\overline{s}^{1/2}\,\overline{x}^{3/2}, \quad 0 < \overline{x} < \infty \tag{42}$$

which becomes unbounded far into the shoaling zone. Because breaking-induced turbulence must diminish away from the surf zone, a different eddy viscosity is assumed that diminishes exponentially with offshore distance from the breaker line

$$\nu = N\rho g^{1/2}\,\overline{s}^{1/2}\,\overline{x}_b^{3/2} e^{-D\left(\overline{x}-\overline{x}_b\right)}, \quad \overline{x}_b < \overline{x} < \infty \tag{43}$$

where D = empirical coefficient. Substituting the expressions for bottom friction [Eq. (40)], radiation stress [Eq. (41)], and eddy viscosities [Eqs. (42) and (43)] in the momentum balance [Eq. (39)] yields

$$\begin{aligned} &r\overline{x}^{3/2} + p_1 \frac{\partial}{\partial \overline{x}}\left(\overline{x}^{5/2}\,\frac{\partial \overline{v}_1}{\partial \overline{x}}\right) - q\overline{x}^{1/2}\,\overline{v}_1 = 0, \quad 0 < \overline{x} < \overline{x}_b \\ &p_2 \frac{\partial}{\partial \overline{x}}\left(\overline{x} e^{-D\overline{x}}\,\frac{\partial \overline{v}_1}{\partial \overline{x}}\right) - q\overline{x}^{1/2}\,\overline{v}_1 = 0, \quad \overline{x}_b < \overline{x} < \infty \end{aligned} \tag{44}$$

where

$$\begin{aligned} &r = \frac{5}{16}\gamma^2 \rho g \overline{s}^{5/2} \sin\theta_b \overline{h}_b^{-1/2}, \quad q = \frac{1}{\pi}\gamma C_f \rho g^{1/2}\,\overline{s}^{1/2}, \\ &p_1 = N\rho g^{1/2}\overline{s}^{3/2}, \quad p_2 = N\rho g^{1/2}\,\overline{s}^{3/2} x_b^{3/2} e^{D\overline{x}_b} \end{aligned} \tag{45}$$

These equations must be solved numerically. The longshore current $\overline{v}_1(\overline{x})$ vanishes at the mean shoreline, $\overline{x} = 0$ and at a distance far offshore. Thus

$$\overline{v}_1 = 0, \quad \overline{x} = 0, \quad \text{and} \quad \infty \tag{46}$$

Continuity of velocity and its derivative is required at the breaker line

$$\lim_{\overline{x} \to \overline{x}_b^-} \overline{v}_1 = \lim_{\overline{x} \to \overline{x}_b^+} \overline{v}_1 \tag{47}$$

$$\lim_{\overline{x} \to \overline{x}_b^-} \frac{\partial \overline{v}_1}{\partial \overline{x}} = \lim_{\overline{x} \to \overline{x}_b^+} \frac{\partial \overline{v}_1}{\partial \overline{x}} \tag{48}$$

The longshore current profile depends on three empirical parameters: N, C_f, and D. The dependency of the longshore current profile on N and C_f has been extensively analyzed in Longuet-Higgins (1970b), who took $0 < N < 0.016$ and $C_f = 0.01$. Tests have been performed herein using different values of N, C_f, and D to best fit the laboratory data by Sun and Tao (2003), which will be presented in the section Comparison with a Laboratory Experiment.

Solute Transport Equation

Using the expressions for the wave velocities [Eq. (27)], the quadratic terms in the transport equation [Eq. (17)] can be readily calculated, and the resulting transport equation becomes

$$\begin{aligned} &\frac{\partial C_0}{\partial \tau} - \alpha \frac{(gkA)^2}{2\omega^3}\frac{\partial C_0}{\partial \overline{x}} + \left[\overline{v}_1 + \beta \frac{(gkA)^2}{2\omega^3}\right]\frac{\partial C_0}{\partial y} \\ &\quad = \frac{1}{\overline{h}}\frac{\partial}{\partial \overline{x}}\left(\overline{h} K_x \frac{\partial C_0}{\partial \overline{x}}\right) + K_y \frac{\partial^2 C_0}{\partial y^2} + \frac{q}{\overline{h}} \end{aligned} \tag{49}$$

In this special case, $\overline{v}_1$ is the longshore current, and the cross-shore current is assumed to be $\overline{u}_1 = 0$. No attempts are made to calibrate the diffusivities K_x and K_y because of lack of reliable data. Thus, Eqs. (42) and (43) are used for the diffusivities. For the boundary conditions, the total mass flux is required to vanish along the shoreline and far outside the surf zone

$$\overline{h} K_x \frac{\partial C_0}{\partial x} = 0, \quad x = -x_s, \text{ and } \infty \tag{50}$$

Interesting physics can be seen in Eq. (49). Because the Stokes drift component β is positive, the solute is advected along the shore at a higher speed than the classical longshore current. In addition, $\alpha > 0$; hence, the solute is also transported toward the shore. If the solute is released outside the breaker line, the advection speeds increase first to a maximum at the breaker line and then diminish to zero at the shoreline. Hence a cloud of contaminants eventually travels close to the shore while spreading laterally by diffusion, as observed in the laboratory and in the field.

The solute transport equation [Eq. (49)] is solved numerically by using the Crank-Nicholson finite-difference scheme with accuracy of order $O(\Delta x^2, \Delta t)$. Convergence and stability tests were performed for different grid sizes. The accuracy of the numerical algorithm was also checked with a known analytical steady-state solution of

J. Waterway, Port, Coastal, Ocean Eng. 2013.139:437-454.

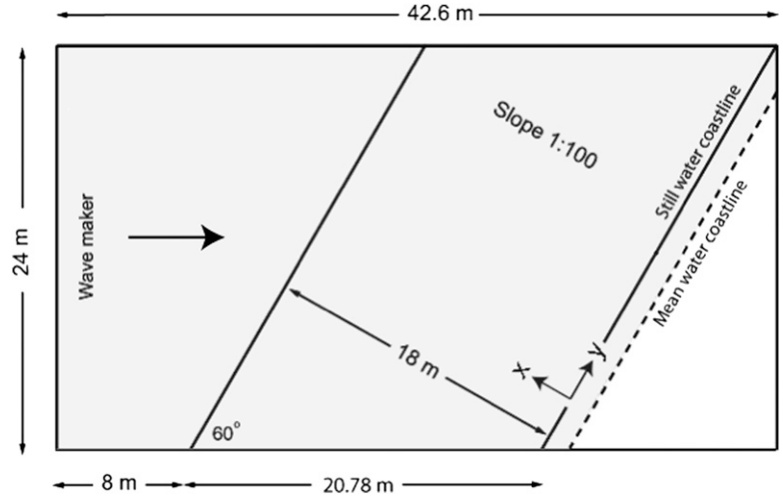

Fig. 3. Plan view of the experimental setup used by Sun and Tao (2003)

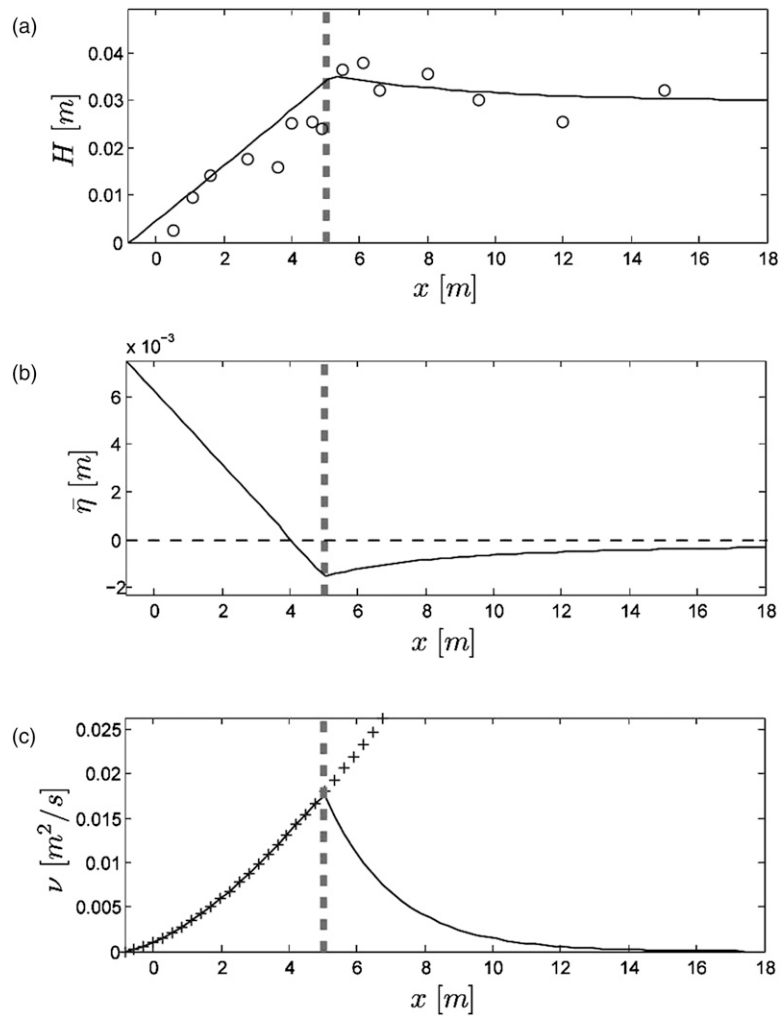

Fig. 4. Wave derived quantities for Test I: (a) model-data comparison of wave heights; circles are experimental data [Fig. 2 in Sun and Tao (2003)] and solid line corresponds to the numerical results (root mean square error between the experimental data and the model is $\epsilon_{\text{rms}} = 0.004$ cm); (b) predicted mean water level in solid line and still water level in thin dotted line; (c) eddy viscosity predicted by the model in solid line and Longuet-Higgins' model, $\nu = Nx\sqrt{gh}$, in crosses; in all plots, dashed gray line indicates the breaker line; wave parameters: $A = 1.5$ cm, $T = 1$ s, $\theta = 30°$, $\gamma = 0.7$, slope $s = 1/100$; longshore current parameters $N = 0.004$, $C_f = 0.0042$, and $D = 0.5\ \text{m}^{-1}$

J. Waterway, Port, Coastal, Ocean Eng. 2013.139:437-454.

concentration from a continuous point source. The analytical solution and its comparisons with numerical results are shown in the Appendix. Further details of several examples related to solute transport inside and outside of a surf zone are presented in the following section.

Comparison with a Laboratory Experiment

Sun and Tao (2003) reported laboratory experiments for longshore current and dye transport. A beach was installed on one side of a basin with horizontal dimensions 40×24 m and a depth of 1.2 m. A sketch of the experimental setup is presented in Fig. 3. Tests were performed for two beach slopes and constant offshore depths: $s = 1/100$ with $h_0 = 18$ cm (Test I), and $s = 1/40$ with $h_0 = 45$ cm (Test II). Dye was released both instantaneously and continuously from the end of a tube close the basin bottom. Hence, the dye concentration was far from uniform in depth, as assumed in the present theory. In their report, only the dye patch shape at one instant was shown for each test, instead of showing the concentration contours at several instants. Nevertheless, the simulations of these tests are described in the hope that extensive and well-controlled experiments will be available in the future for more definitive comparisons.

Qualitative Model-Data Comparison for 1/100 Slope (Test I)

The incident regular wave conditions at the offshore boundary for Test I were as follows: amplitude $A = 1.5$ cm, wave period $T = 1$ s, and angle of incidence $\theta = 30°$. In the present coordinate system, the toe of the beach was located at $x = 18$ m. Fig. 4(a) shows that the predicted wave height ($H = 2A$) agrees well with the measured data [Fig. 2 in Sun and Tao (2003)], with a root mean square error of $\epsilon_{\text{rms}} = 0.004$ cm. The predicted mean free surface is plotted in Fig. 4(b), but no experimental data are available for comparison. The numerical results show that the breaker line is located at $x = x_b = 5$ m, whereas the mean shoreline is at $x = -x_s = -0.74$ m. Fig. 4(c) displays the eddy viscosity calculated from Eqs. (42)

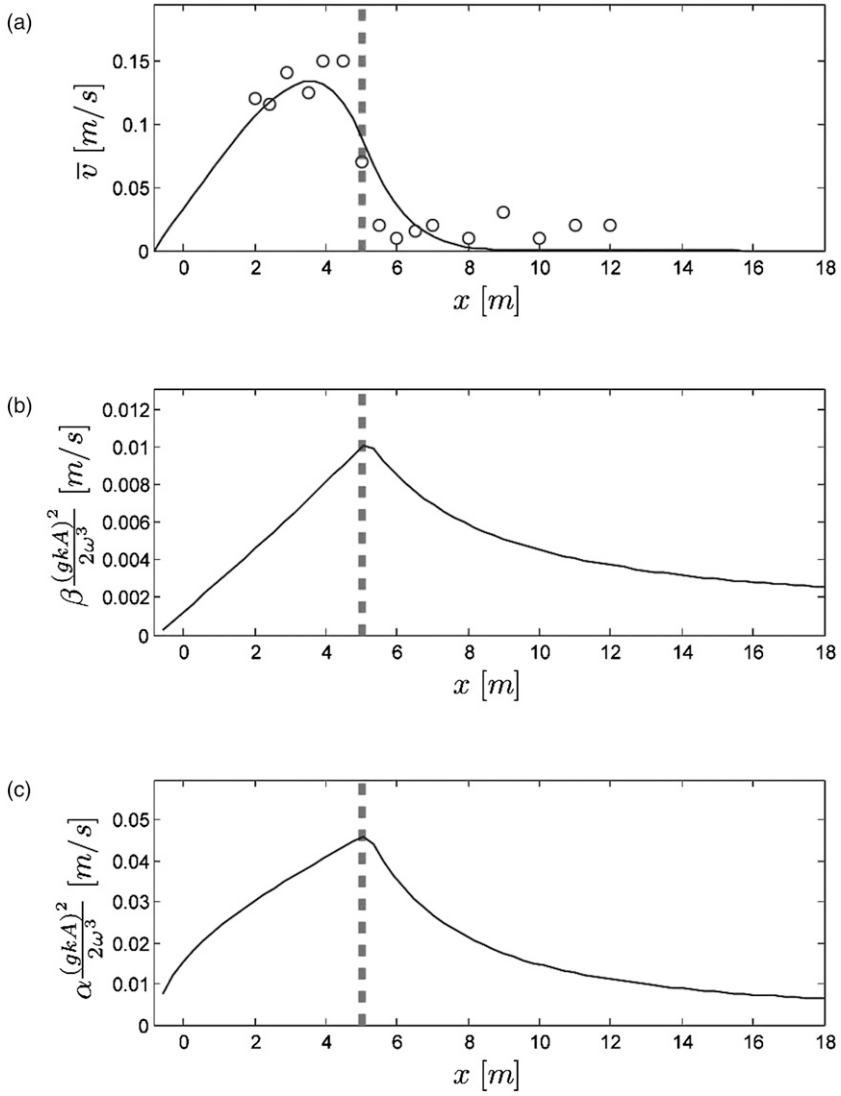

Fig. 5. Currents for Test I: (a) model-data comparison of longshore current; circles are experimental data [Fig. 2 in Sun and Tao (2003)] and solid line corresponds to the numerical results (root mean square error between the experimental data and the model is $\epsilon_{\text{rms}} = 0.019$ m/s); (b) predicted longshore Stokes drift velocity; (c) predicted cross-shore Stokes drift velocity; in all plots, dashed gray line indicates the breaker line; wave parameters: $A = 1.5$ cm, $T = 1$ s, $\theta = 30°$, $\gamma = 0.7$, slope $s = 1/100$; longshore current parameters: $N = 0.004$, $C_f = 0.0042$, and $D = 0.5$ m^{-1}

J. Waterway, Port, Coastal, Ocean Eng. 2013.139:437-454.

and (43), with $N = 0.004$, $C_f = 0.0042$, $D = 0.5\,\mathrm{m}^{-1}$, and a breaking index of $\gamma = 0.7$. The maximum value at the breaker line is $\nu_{\max} = 0.17\,\mathrm{m}^2/\mathrm{s}$.

The predicted longshore current in Fig. 5(a) peaks at $v_{\max} = 0.135\,\mathrm{m/s}$ and fits the experimental data [Fig. 3 in Sun and Tao (2003)] with a root mean square error of $\epsilon_{\mathrm{rms}} = 0.019\,\mathrm{m/s}$. The theoretical longshore and cross-shore Stokes drift velocities, $\alpha(gkA)^2/2\omega^3$ and $\beta(gkA)^2/2\omega^3$, are shown in Figs. 5(b and c), respectively. The longshore component of the Stokes drift is much smaller than the longshore current, whereas the cross-shore Stokes drift is about one-half of the longshore current. All parameters depicted in Figs. 4 and 5 are used to compute the leading order concentration C_0 [Eq. (49)] for both the instantaneous and continuous releases in Test I.

Mixing Pattern for Instantaneous Source

For the instantaneous release, numerical simulations were carried out in a domain of $18 \times 18\,\mathrm{m}$ in the cross-shore and longshore directions to cover the entire slope in Fig. 3. The spatial grid size was set to $\Delta x = \Delta y = 0.28\,\mathrm{m}$, and the time step was $\Delta t = 1\,\mathrm{s}$. The source was modeled by a Gaussian cloud [Eq. (22)], with a nondimensional peak value of $\tilde{C}_{\max} = 1$ at $(x_0, y_0) = (4.5, 2.0\,\mathrm{m})$. Having no detailed information on the release, SDs were arbitrarily set to $\sigma_x = \sigma_y = 0.56\,\mathrm{m}$.

In Sun and Tao (2003), only one test result was reported for instantaneous release under regular waves on a slope of $s = 1/100$, where the dye release was just inside the breaker line. One snapshot of the dye cloud was photographed at 50 s after the initial release [Fig. 6 in Sun and Tao (2003)]. Fig. 6(a) shows contour lines

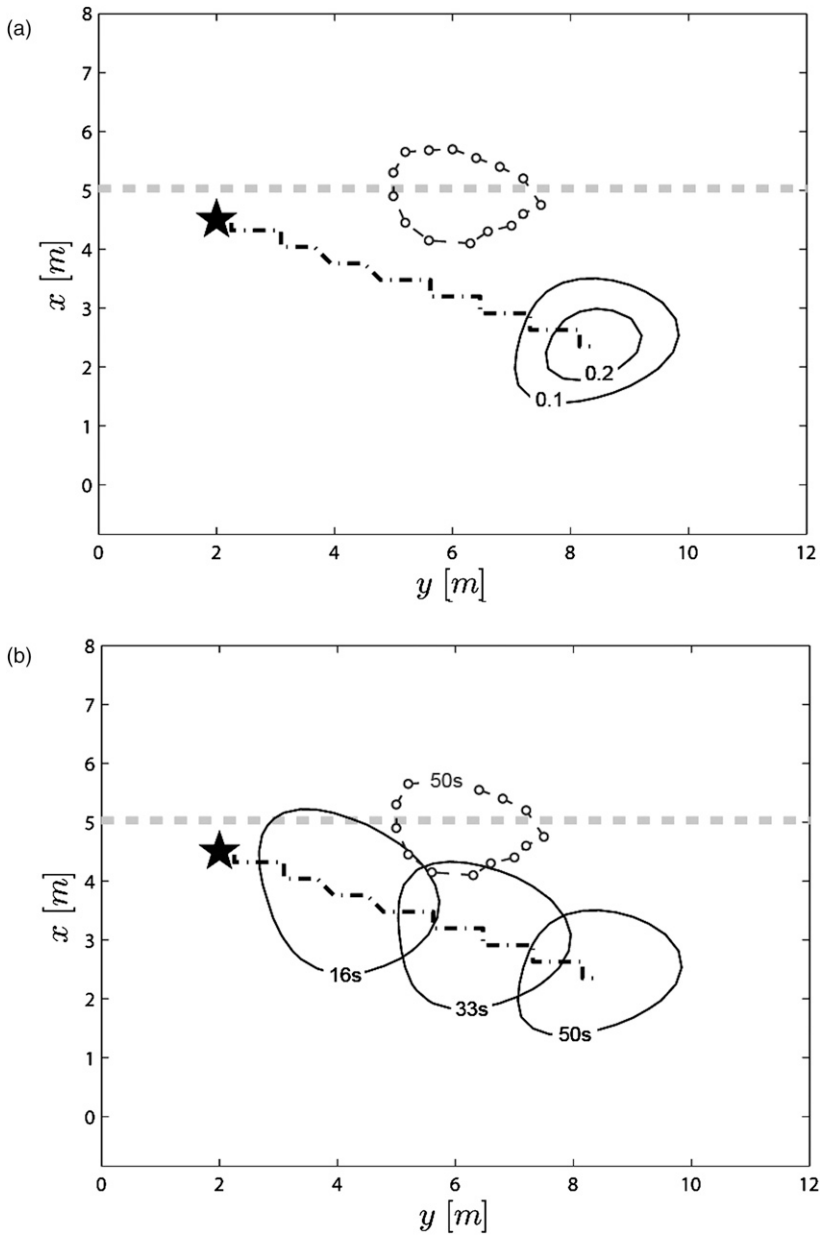

Fig. 6. Mixing of instantaneous release for Test I: (a) experimental results at 50 s are shown by dotted lines [Fig. 6 in Sun and Tao (2003)], and numerical results are shown by solid lines; (b) time evolution of the isocontour $C_0 = 0.1$ at 16, 33, and 50 s (star depicts the location of release and the dashed gray line indicates the breaker line; dashed-dotted line corresponds to the trajectory of the maximum concentration); wave parameters: $A = 1.5\,\mathrm{cm}$, $T = 1\,\mathrm{s}$, $\theta = 30°$, $\gamma = 0.7$, slope $s = 1/100$; longshore current parameters: $N = 0.004$, $C_f = 0.0042$, and $D = 0.5\,\mathrm{m}^{-1}$

of the dye cloud 50 s after the instantaneous release. The cloud is significantly advected downstream, and the concentration distribution slightly deviates from the initial Gaussian shape. Fig. 6(b) depicts the time evolution of the cloud by means of three snapshots of numerical results for the concentration contour $C_0 = 0.1$ at $t = 16, 33,$ and 50 s. As predicted by Eq. (49), the computed cloud drifts both shoreward and alongshore, being elongated rapidly in the longshore direction as a consequence of the much smaller cross-shore current velocity.

The observed dye movement is much slower than the drifting fluid for the experimental data. Because the predicted longshore velocity agrees well with the measurement, the difference in the observed dye movement could be explained in part be because of the proximity of the release point to the basin bottom, where velocities

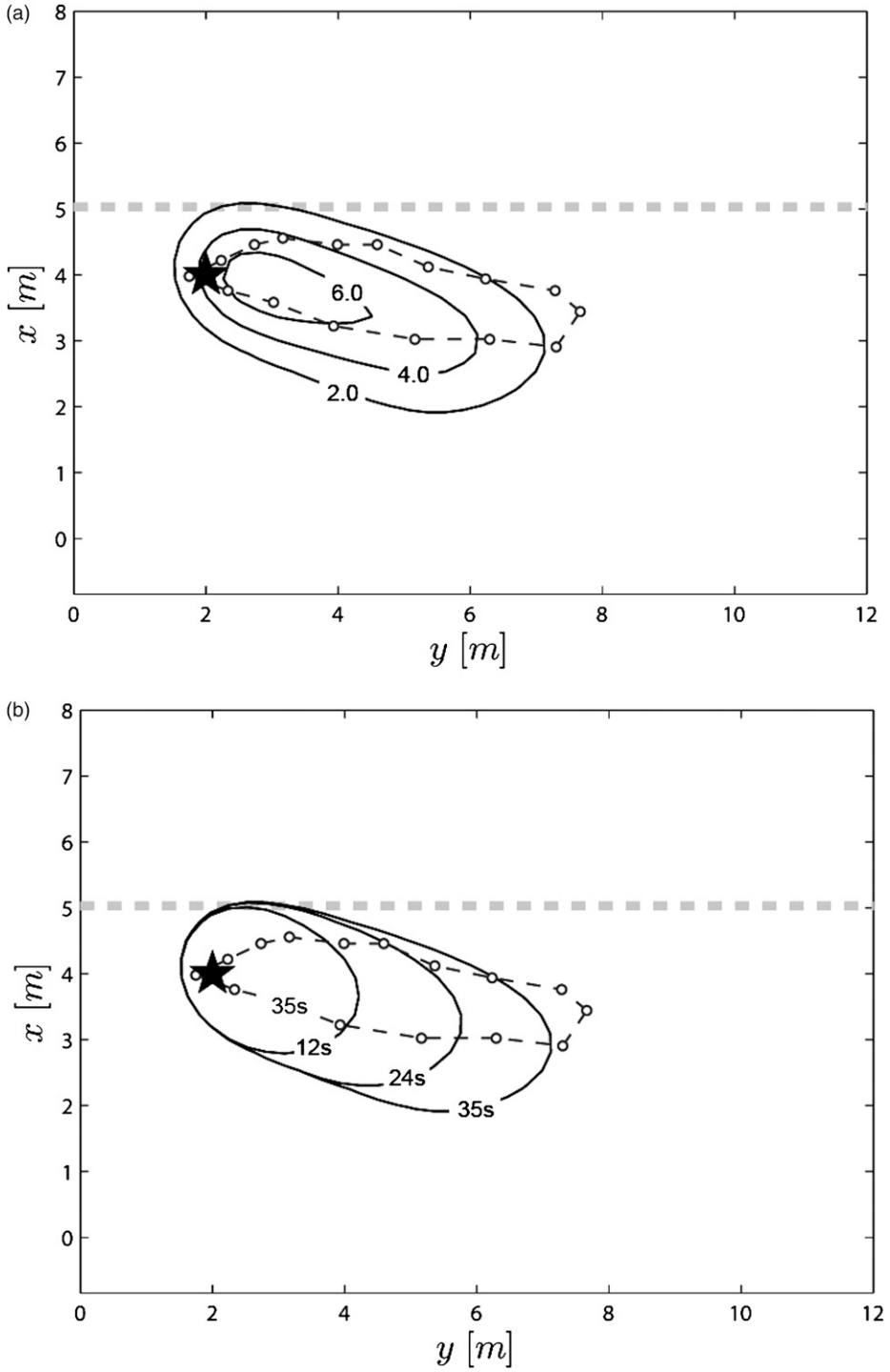

Fig. 7. Mixing of continuous release for Test I: (a) experimental results at 35 s are shown by dotted lines [Fig. 7 in Sun and Tao (2003)] and numerical results are shown by solid lines; (b) time evolution of the isocontour $C_0 = 2.0$ at 12, 24, and 35 s (star depicts the location of release and the dashed gray line indicates the breaker line); wave parameters: $A = 1.5$ cm, $T = 1$ s, $\theta = 30°$, $\gamma = 0.7$, slope $s = 1/100$; longshore current parameters: $N = 0.004$, $C_f = 0.0042$, and $D = 0.5\,\mathrm{m}^{-1}$

J. Waterway, Port, Coastal, Ocean Eng. 2013.139:437-454.

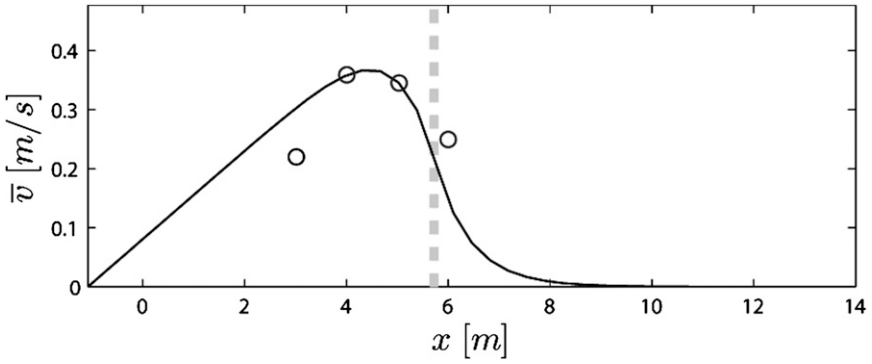

Fig. 8. Longshore currents used to adjust coefficients N, C_f, and D for Test II: longshore current from experiments by Tao and Han (2002) is plotted in circles [Fig. 3 in Tao and Han (2002)], and the calculated profile used for calibration of slope $1/40$ is shown by solid lines; root mean square error between the experimental data and the model is $\epsilon_{\text{rms}} = 0.065$ m/s; dashed gray line represents the breaker line; wave parameters: $A = 5.12$ cm, $T = 1.4$ s, $\theta = 30°$, $\gamma = 0.7$, slope $s = 1/40$; longshore current parameters: $N = 0.001$, $C_f = 0.009$, and $D = 0.01$ m^{-1}

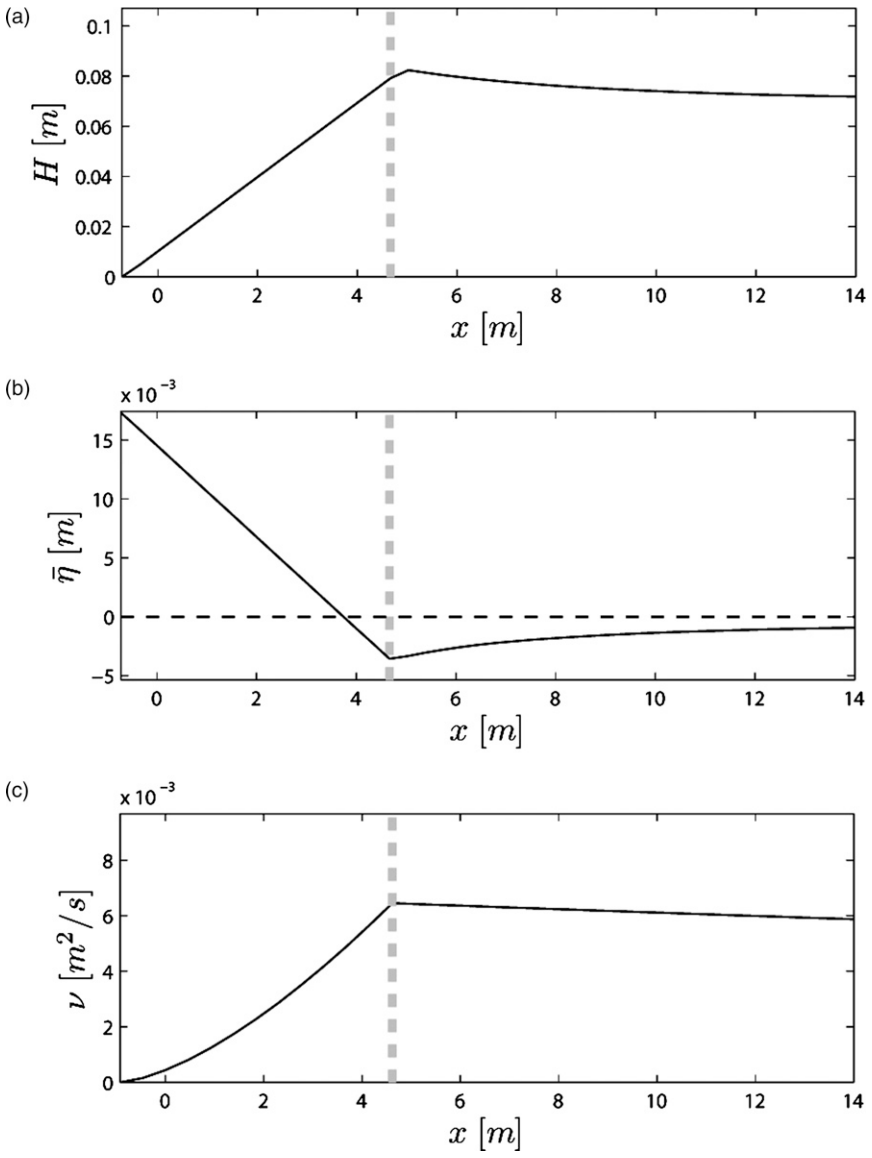

Fig. 9. Wave-derived quantities for Test II: (a) predicted wave heights for the continuous release (Sun and Tao 2003); (b) predicted mean water level in solid line and still water level in thin dotted line; (c) predicted eddy viscosity; in all plots, dashed gray line indicates the breaker line; wave parameters: $A = 4.0$ cm, $T = 1.5$ s, $\theta = 30°$, $\gamma = 0.7$, slope $s = 1/40$; longshore current parameters: $N = 0.001$, $C_f = 0.009$, and $D = 0.01$ m^{-1}

J. Waterway, Port, Coastal, Ocean Eng. 2013.139:437-454.

are smaller than in the surface. Unfortunately, no further details on vertical patterns are available (e.g., mechanism used to released the solute, vertical profile of the horizontal velocities and concentration), and no other records are presented in the original paper to show the repeatability of the data. A conclusive explanation of the difference between flow and cloud velocities is thus not possible.

Mixing Pattern for Continuous Source

Numerical simulations were carried out using the same grid and time step used for the instantaneous release ($\Delta x = \Delta y = 0.28$ m and $\Delta t = 1$ s). The source was modeled by a 2D Gaussian cloud with a peak value for the rate of discharge per unit area of $\tilde{Q}_{\max} = 1\ \mathrm{ms}^{-1}$, centered at $(x_0, y_0) = (4.0\,\mathrm{m}, 2.0\,\mathrm{m})$, with arbitrarily chosen SDs of $\sigma_x = \sigma_y = 0.56$ m.

Fig. 7(a) shows the predicted concentration contours at 35 s after the initiation of the release. The concentrations remain high near the source as a consequence of the continuous release of solute and decay far from the source because of both advection and diffusion. Fig. 7(b) displays the time evolution of the dye cloud by means of three snapshots of the concentration contour $C_0 = 2.0$ at $t = 12, 24$, and 35 s. The computed cloud drifts both shoreward and alongshore and has an elongated shape in the longshore direction. From the experiment, only the outer boundary of the dye cloud at $t = 35$ s was available [Fig. 7 in Sun and Tao (2003)] and is included here for comparison. Although the numerical cloud drifts slightly more onshore, both the trajectory and shape are quite similar to the observed dye cloud, suggesting a qualitative confirmation of the theory.

Qualitative Model-Data Comparison for a 1/40 Slope (Test II)

Sun and Tao (2003) also reported observations of dye transport on the 1/40 slope for both the instantaneous and continuous releases [Figs. 12 and 13 in Sun and Tao (2003)]. For the instantaneous source, neither longshore current nor wave height measurements were reported in the region where mixing occurs. For the continuous release case, only the incident wave conditions at the offshore boundary were available, and no data on wave shoaling and longshore currents were reported. Therefore, another set of experiments by Tao and Han (2002) in the same facility is used to tune coefficients determining the longshore currents. Numerical simulations of their laboratory observations under irregular waves with the mean amplitude $\overline{A} = 4.0$ cm, mean period $\overline{T} = 1.5$ s, and

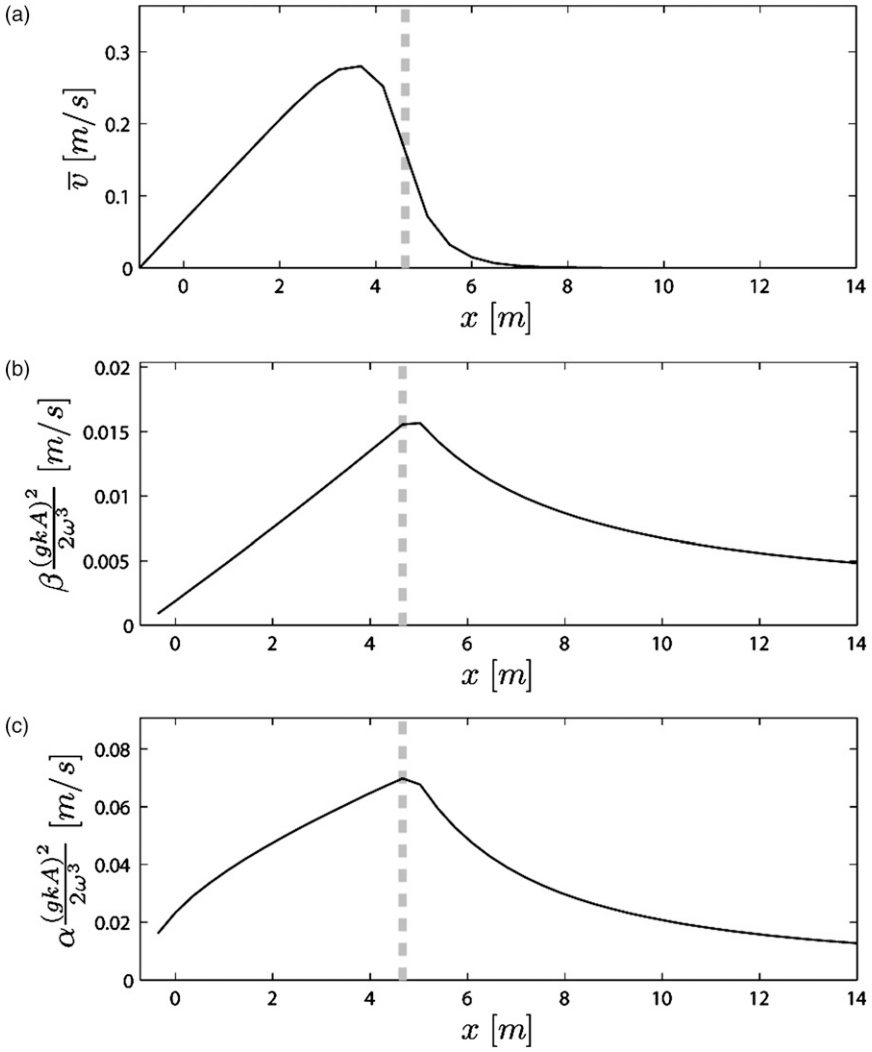

Fig. 10. Currents for Test II: (a) predicted longshore current; (b) predicted longshore Stokes drift velocity; (c) predicted cross-shore Stokes drift velocity; in all plots dashed gray line indicates the breaker line; wave parameters: $A = 4.0$ cm, $T = 1.5$ s, $\theta = 30°$, $\gamma = 0.7$, slope $s = 1/40$; longshore current parameters: $N = 0.001$, $C_f = 0.009$, and $D = 0.01\ \mathrm{m}^{-1}$

J. Waterway, Port, Coastal, Ocean Eng. 2013.139:437-454.

angle of incidence $\theta = 30°$ are reported. As a first approximation, the random waves are modeled by regular waves with the same mean wave amplitude and wave period.

The parameters used for calculating the longshore current (N, C_f, D, and γ) were obtained by matching the numerical solutions with the longshore current measurements in the same facility reported in Tao and Han (2002) for regular waves with amplitude of $A = 5.12\,\text{cm}$, wave period of $T = 1.4\,\text{s}$, and angle of incidence $\theta = 30°$ on a $1/40$ slope. Fig. 8 shows the comparison between the theoretical solution for longshore current and the experimental data [Fig. 3 in Tao and Han (2002)], using $N = 0.001$, $C_f = 0.009$, $D = 0.01\,\text{m}^{-1}$, and a breaking index of $\gamma = 0.7$. The root mean square error between the experimental velocities and the model is $\epsilon_{\text{rms}} = 0.65\,\text{m/s}$, which is relatively high compared with the actual values of velocity.

Using these coefficients and the incident wave conditions ($\overline{A} = 4.0\,\text{cm}$, $\overline{T} = 1.5\,\text{s}$, and $\theta = 30°$), the wave height, mean water level and eddy viscosity (Fig. 9), longshore current, and Stokes drift velocity components (Fig. 10) are calculated. These parameters are used to compute the leading order concentration C_0 using the governing equation [Eq. (49)] for the continuous release in Test II.

The release was modeled by a Gaussian cloud with a peak value for the rate of discharge per unit area of $\tilde{Q}_{\max} = 1\,\text{ms}^{-1}$ at $(x_0, y_0) = (3.0\,\text{m}, 2.0\,\text{m})$, with arbitrarily chosen SDs of $\sigma_x = \sigma_y = 0.56\,\text{m}$, as defined in Eq. (22). Fig. 11 depicts the position of the dye cloud at 30 s after the initiation of the release [Fig. 13 in Sun and Tao (2003)], and its evolution is based on the numerical results at $t = 10$, 20, and 30 s. Both the experimental and numerically simulated dye clouds show comparable drift angles and patch sizes, although the numerical results tend to be slightly further onshore.

Field-Scale Examples by Computation

To gain further understanding of the physics of solute transport on the field scale, a hypothetical case was examined in which wave conditions are typical of those on a beach exposed to swells. The numerical simulations were carried out on a plane beach of slope $s = 1/100$, extending to infinity alongshore and to deep water in the cross-shore direction.

The following wave conditions at the offshore boundary in deep waters were chosen: amplitude $A = 0.5\,\text{m}$, period $T = 10\,\text{s}$, and angle of incidence $\theta = 30°$. Wave propagation was carried out toward shallow waters using the linear wave theory and Snell's law.

Fig. 12(a) shows the surf-zone wave height, and the mean free surface is plotted in Fig. 12(b). The breaker line is located at $x = x_b = 61.4\,\text{m}$, whereas the mean shoreline is located at $x = -x_s = -9.1\,\text{m}$. Fig. 12(c) displays the eddy viscosity profile calculated with $N = 0.002$, $C_f = 0.01$, $D = 0.1\,\text{m}^{-1}$, and $\gamma = 0.7$. The parameters N and C_f were extracted from Longuet-Higgins (1970a, b), and D was arbitrarily chosen. The breaker coefficient adopted herein is consistent with the literature (Svendsen 2006; Longuet-Higgins 1970a). The resulting eddy viscosity (i.e., diffusivity) is of order $\mathcal{O}(1)\,\text{m}^2/\text{s}$, agreeing with the range of values reported by Takewaka et al. (2003), Mariani (2004), and Clark et al. (2010). The maximum eddy viscosity at the breaker line is $\nu_{\max} = 0.67\,\text{m}^2/\text{s}$.

The longshore current profile is depicted in Fig. 13(a), and the maximum velocity is $\overline{v}_{\max} = 0.7\,\text{m/s}$. Longshore and cross-shore Stokes drift velocities are shown in Figs. 13(b and c), with maximum values of 0.036 and 0.27 m/s, respectively. Similar to the laboratory cases, the longshore component of the Stokes drift velocity is much smaller than the calculated longshore current velocity, whereas the cross-shore component is about one-half of the longshore current. Hence, the center of a solute cloud drifts to the shore while moving downstream along the shore.

Mixing Pattern for Instantaneous and Continuous Sources

Numerical simulations for instantaneous and continuous dye releases up to 150 s were carried out in a domain of $150 \times 300\,\text{m}$ in

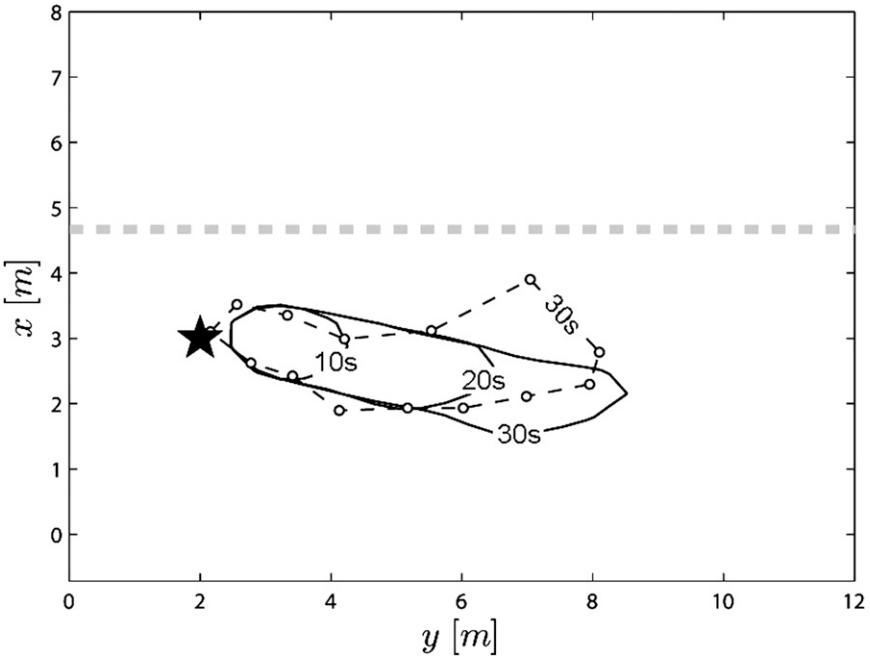

Fig. 11. Mixing of continuous release for Test II: experimental results at 30 s are shown by dotted lines [Fig. 13 in Sun and Tao (2003)] and the numerical results at 10, 20, and 30 s are plotted by solid lines (star depicts the location of release, and the dashed gray line indicates the breaker line); wave parameters: $A = 4.0\,\text{cm}$, $T = 1.5\,\text{s}$, $\theta = 30°$, slope $s = 1/40$; longshore current parameters: $N = 0.001$, $C_f = 0.009$, and $D = 0.01\,\text{m}^{-1}$

J. Waterway, Port, Coastal, Ocean Eng. 2013.139:437-454.

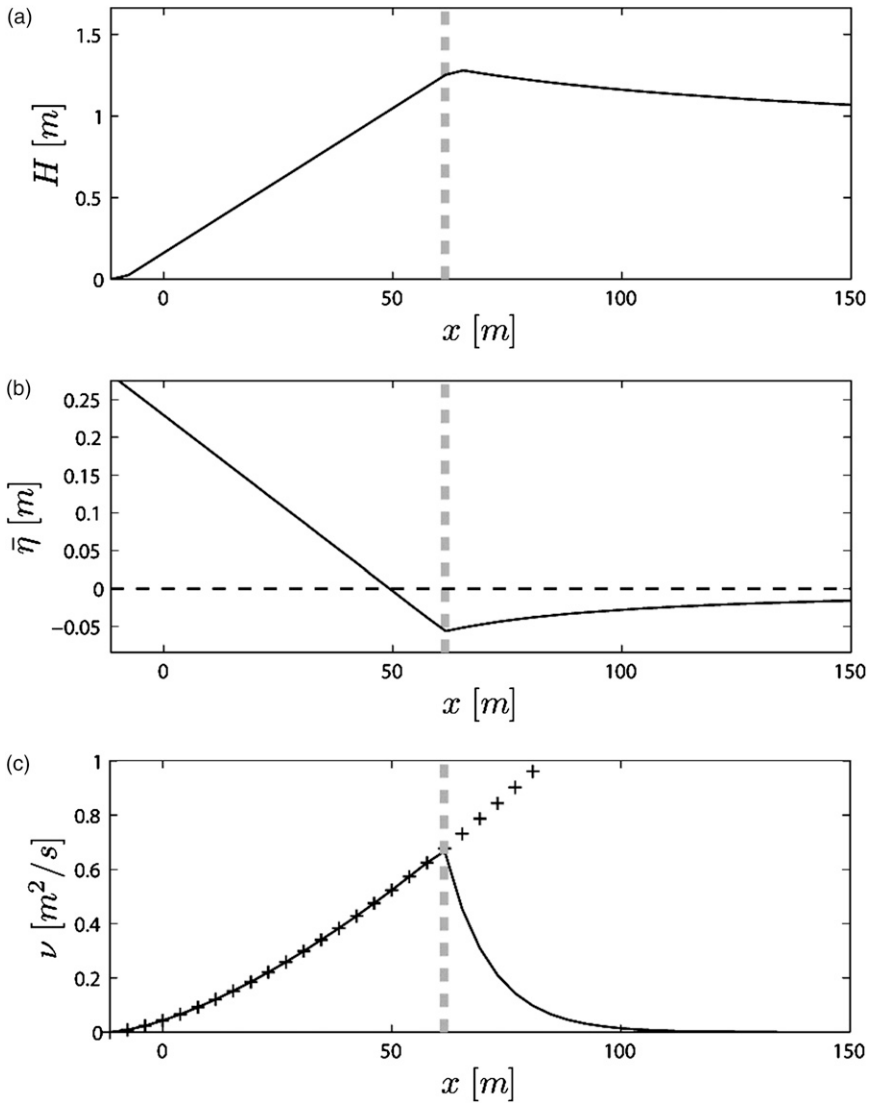

Fig. 12. Wave-derived quantities for field scale example: (a) predicted wave heights; (b) predicted mean water level in solid line and still water level in thin dotted line; (c) eddy viscosity predicted by the model in solid lines and Longuet-Higgins' model, $\nu = Nx\sqrt{gh}$, in crosses; in all plots dashed gray line indicates the breaker line; wave parameters: $A = 0.5$ m, $T = 10$ s, $\theta = 30°$, $\gamma = 0.7$, slope $s = 1/100$; longshore current parameters: $N = 0.002$, $C_f = 0.01$, and $D = 0.1\ \mathrm{m}^{-1}$

the cross-shore and longshore directions, respectively. The spatial grid size was $\Delta x = \Delta y = 3.84$ m, and the time step was $\Delta t = 1$ s. The source was modeled by a Gaussian cloud with a nondimensional peak value of concentration of $\tilde{C}_{\max} = 1$ for the instantaneous case and a maximum rate of discharge per unit area of $\tilde{Q}_{\max} = 1\ \mathrm{ms}^{-1}$ for the continuous case. SDs of $\sigma_x = \sigma_y = 6.14$ m were arbitrarily used in both cases. Three release positions were tested: within the surf zone ($x_0 = 40$ m, $y_0 = 50$ m); slightly seaward of the breaker line ($x_0 = 80$ m, $y_0 = 50$ m), and farther offshore of the the breaker ($x_0 = 120$ m, $y_0 = 50$ m). Concentration contours at $t = 100, 200$, and 300 s are depicted in Figs. 14 and 15 for the instantaneous and continuous cases, respectively. When the dye is released outside the surf zone and far away from the breaker [$x_0 = 120$ m; Figs. 14(a) and 15(a)], the dye patch moves slowly in the shoaling zone because the longshore current and Stokes drift velocities are both weak. However, as the cloud reaches the breaker line, the effects of diffusion and advection grow because of the increasing diffusivities, Stokes drift, and longshore current. When dye is released close to the breaker line [$x_0 = 80$ m; Figs. 14(b) and 15(b)], the cloud is advected at a much higher current speed along the surf zone. As a consequence, the solute is elongated and widened by a combination of diffusion and enhanced longshore advection; thus, concentrations are quickly reduced. For a release near the shoreline [$x_0 = 40$ m; Figs. 14(c) and 15(c)], the early evolution has a similar pattern, but later, the cloud clings close to the shoreline where diffusion and longshore movement slow down because the diffusivity, longshore, and wave-driven velocities go to zero at the shore.

Travel Distance for a Continuous Plume to Reach the Shore

Next, the travel distance for the peak of a continuously released pollutant plume to reach the shoreline from the source was examined. The distance between the source and this point of contact (i.e., landing) is referred to as contact distance and denoted by L_{contact} in Fig. 16(a). Dependence of the contact distance on the source position, local wave conditions, and bathymetry is useful for the

J. Waterway, Port, Coastal, Ocean Eng. 2013.139:437-454.

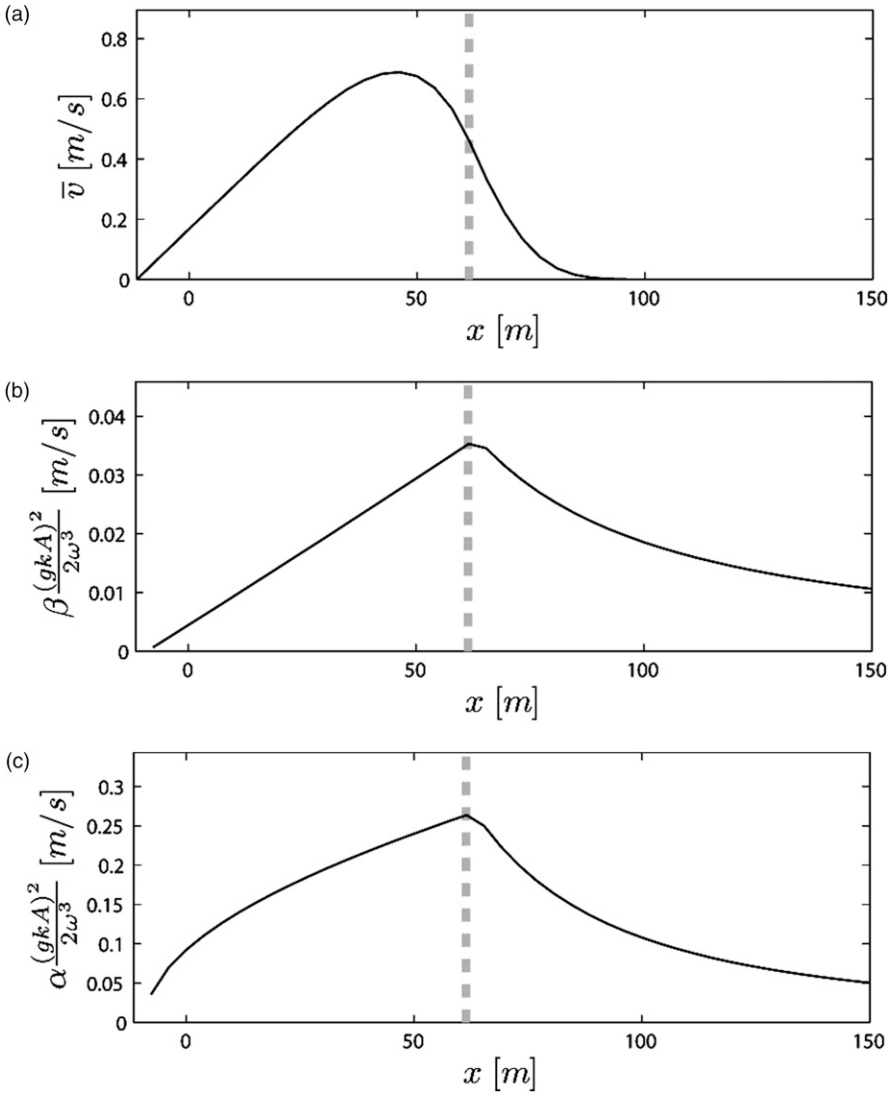

Fig. 13. Currents for field scale example: (a) predicted longshore current; (b) predicted longshore Stokes drift velocity; (c) predicted cross-shore Stokes drift velocity; in all plots dashed gray line indicates the breaker line; wave parameters: $A = 0.5$ m, $T = 10$ s, $\theta = 30°$, $\gamma = 0.7$, slope $s = 1/100$; longshore current parameters: $N = 0.002$, $C_f = 0.001$, and $D = 0.1\ \mathrm{m}^{-1}$

design of marine outfalls or safety issues during spills, among other applications. The analysis is intended to give a taste of the orders of magnitudes and trends of this quantity for some typical wave conditions, without going through a detailed sensitivity analysis.

Using the same Gaussian source with ($\sigma_x = \sigma_y = 6.14$ m) and $\tilde{Q}_{\max} = 1$, the contact distances for a wide range of incident angles and periods are computed. Only two different values of release position, beach slope, and wave amplitude are considered.

In Figs. 16(b–e), each curve is the contour of equal contact distance for a fixed set of source position x_0, offshore wave amplitude A, and beach slope s. Each pair of wave period T and incidence angle θ corresponds to a point in the plot, from which the contact distance in meters is given by the intersecting contour. As expected, for any fixed set of (x_0, A, s), the contact distance increases with the angle of incidence—being zero for normal incidence with $\theta = 0°$—and decreases with increasing wave period as a consequence of refraction. By comparing Figs. 16(b and c), the contact distance increases with the slope, because in the latter ($s = 1/40$), waves feel the bottom closer to the shoreline and deflection of the wave fronts is less significant. For the same release point and beach slope, the contact distance increases slightly with the offshore wave amplitude, as seen by comparing Figs. 16(b and d). However, the distance is nearly doubled if the release point is twice as far offshore, as shown in Figs. 16(b and e).

Concluding Remarks

Using the same assumptions as those in existing theories for the longshore current, the advective diffusion equation for the transport and spreading of solute in the surf zone is derived. The total advection velocity is found to be the sum of the steady current caused by radiation stresses and a contribution from the covariance of fluctuating velocity and concentration. The latter contribution has been ignored by many existing models for analyzing solute transport in the surf zone. The solute transport [Eq. (17)] can be applied to complex bathymetries and wave conditions. In Eq. (49), Stokes drift contributes to the convection velocity in both

J. Waterway, Port, Coastal, Ocean Eng. 2013.139:437-454.

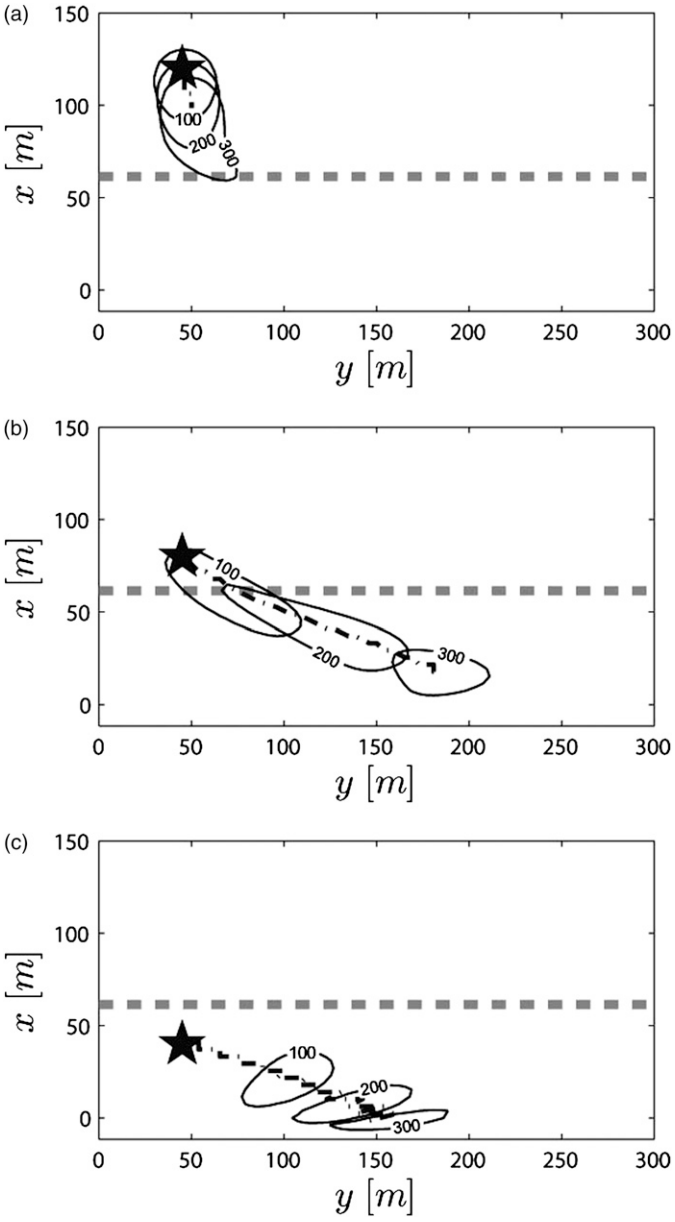

Fig. 14. Time evolution of instantaneous releases for field-scale example at positions: (a) $x_0 = 40$ m; (b) $x_0 = 80$ m; and (c) $x_0 = 120$ m for $t = 100, 200$, and 300 s (star depicts the location of release and the dashed gray line indicates the breaker line): the contour line corresponds to $C_0 = 0.1$; the dashed-dotted line corresponds to the trajectory of the maximum concentration; wave parameters: $A = 0.5$ m, $T = 10$ s, $\theta = 30°$, $\gamma = 0.7$, slope $s = 1/100$; longshore current parameters: $N = 0.002$, $C_f = 0.01$, and $D = 0.1\ \mathrm{m}^{-1}$

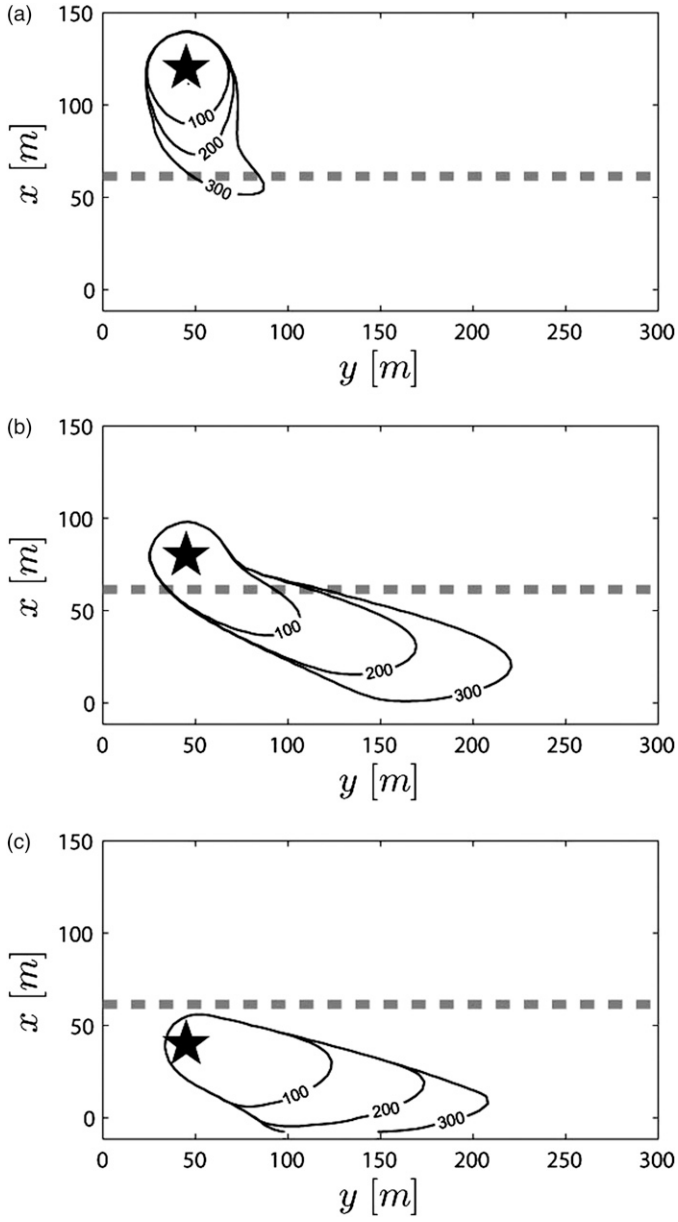

Fig. 15. Time evolution of continuous releases for field-scale example at positions: (a) $x_0 = 40$ m; (b) $x_0 = 80$ m; and (c) $x_0 = 120$ m for $t = 100, 200$, and 300 s (star depicts the location of release and the dashed gray line indicates the breaker line): the contour line corresponds to $C_0 = 2.0$; wave parameters: $A = 0.5$ m, $T = 10$ s, $\theta = 30°$, $\gamma = 0.7$, slope $s = 1/100$; longshore current parameters: $N = 0.002$, $C_f = 0.01$, and $D = 0.1\ \mathrm{m}^{-1}$

cross-shore and longshore directions, represented by $\alpha(gkA)^2/2\omega^3$ and $\beta(gkA)^2/2\omega^3$, which are proportional to the square of the wave steepness. It is demonstrated that pollutants being released in the surf zone will eventually reach the shoreline and stay at the shoreline. With proper estimates of empirical parameters, the present theory can simulate the location and period-averaged concentration of the pollutant along the shoreline. Attempts are made to compare the numerical simulations with available experiments with partial success. Because of the lack of information on the initial conditions, experimental setup, and actual values of the concentration, comparisons remain qualitative, and no identification of the sources of errors or limitations of the theory is attempted. Definitive comparison calls for more comprehensive data in well-controlled and more thoroughly documented tests in the laboratory.

Appendix. Final State of Continuous Source

In this appendix, the analytical steady solution for a concentration distribution generated by a continuous release at a point source in a unidirectional constant flow is shown. The analytical solution is then used to check the numerical algorithm used in this paper.

J. Waterway, Port, Coastal, Ocean Eng. 2013.139:437-454.

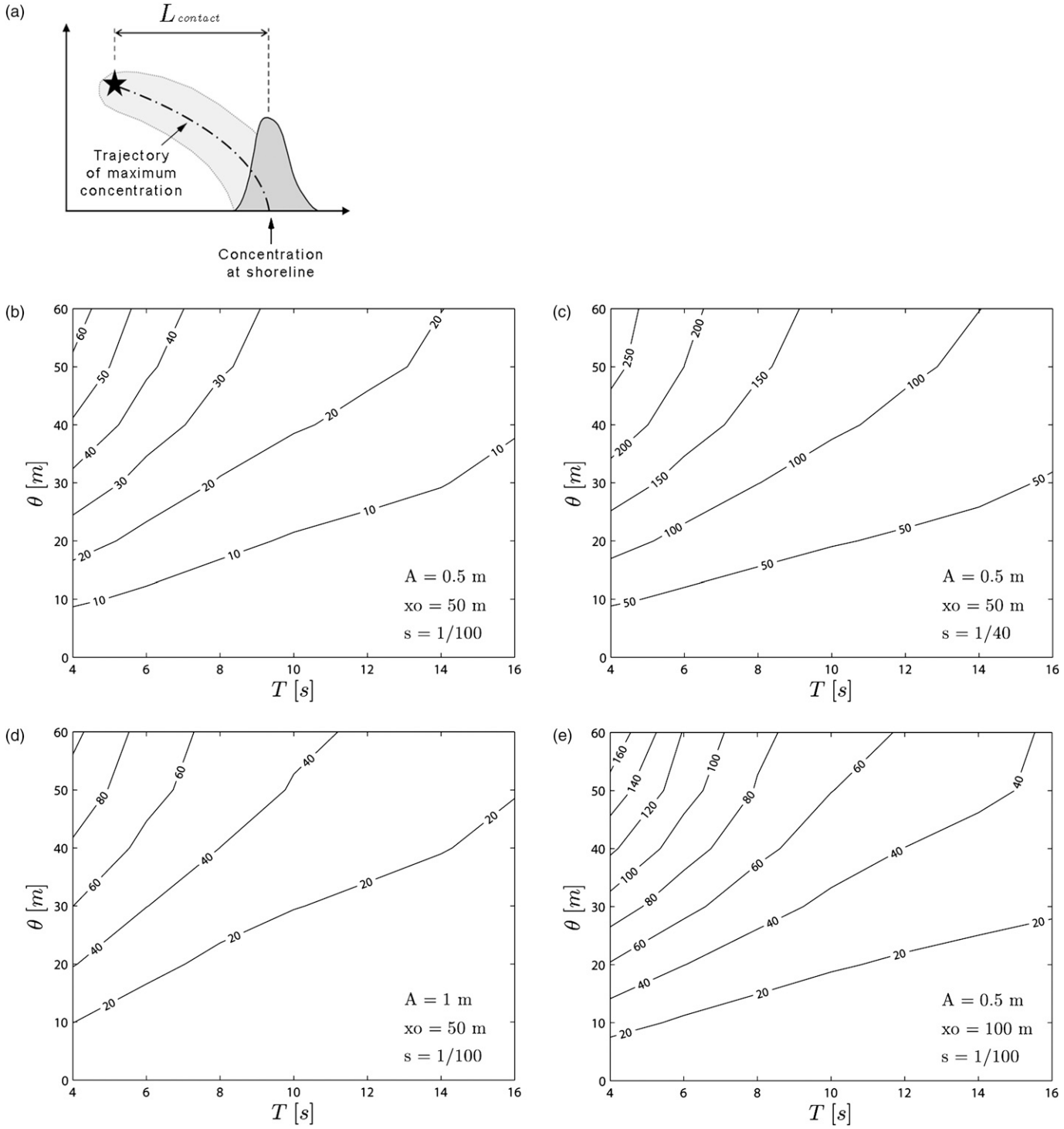

Fig. 16. Contact distances for the field-scale example: (a) schematics defining the contact distance L_{contact}; (b) isocontours of contact distance in meters, for offshore wave amplitude $A = 0.5$ m, slope $s = 1/100$, and release point $x_0 = 50$ m; (c) isocontours for $A = 0.5$ m, $s = 1/40$, and $x_0 = 50$ m; (d) isocontours for $A = 1.0$ m, $s = 1/100$, and $x_0 = 50$ m; (e) isocontours for $A = 0.5$ m, $s = 1/100$, and $x_0 = 100$ m; wave parameters: periods in the range $T = 4-16$ s, offshore angle of incidence in the range $\theta = 0-40°$, $\gamma = 0.7$; longshore current parameters: $N = 0.002$, $C_f = 0.01$, and $D = 0.1\ \text{m}^{-1}$

Consider a steady-state condition, $\partial/\partial\tau = 0$, a flow of constant depth, and constant and isotropic diffusivity. The simplified transport equation becomes

$$v\frac{\partial C}{\partial y} = K\left(\frac{\partial^2 C}{\partial x^2} + \frac{\partial^2 C}{\partial y^2}\right) + \frac{Q_0}{h_o}\delta(x)\delta(y) \tag{51}$$

where h_o = depth at the source. The boundary conditions require

$$C \to 0, \quad x, y \to \pm\infty \tag{52}$$

Take Fourier transform

J. Waterway, Port, Coastal, Ocean Eng. 2013.139:437-454.

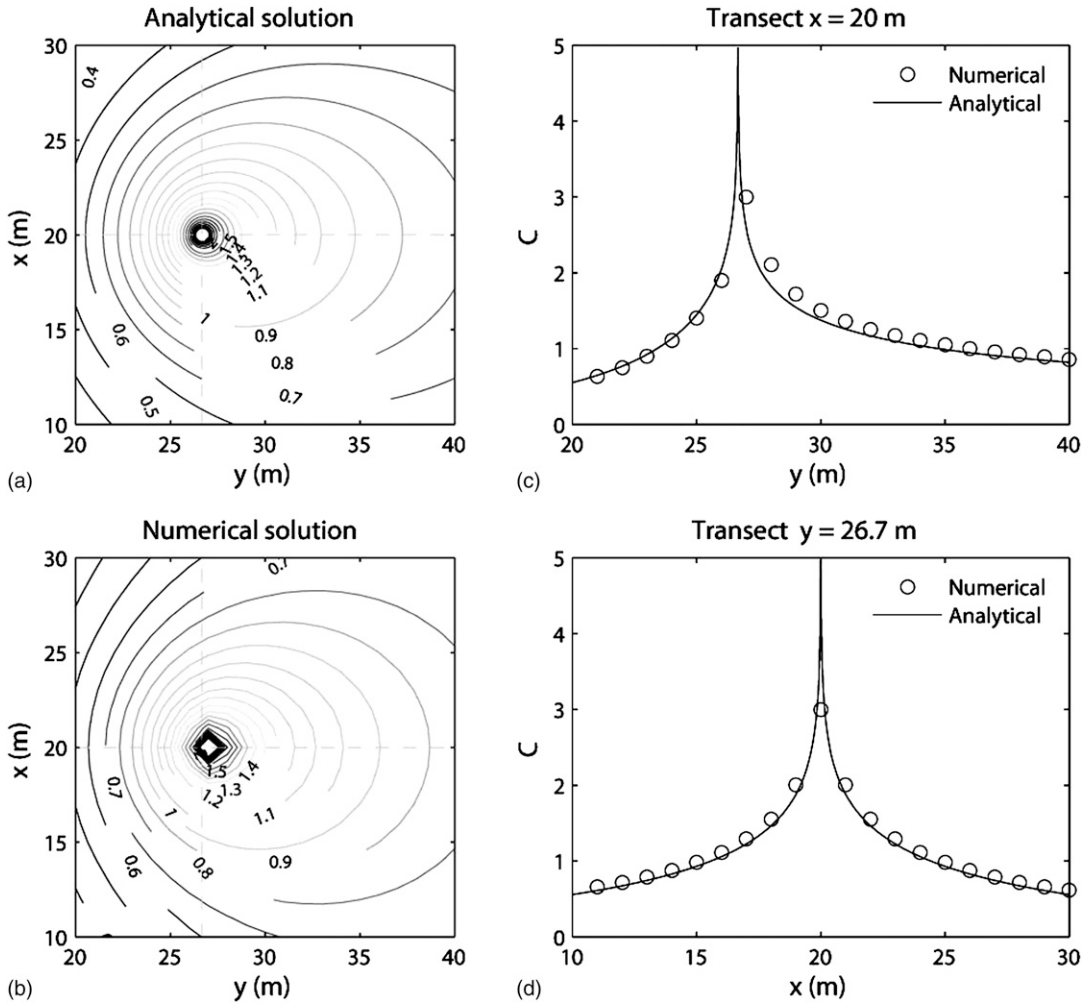

Fig. 17. (a and b) Analytical and numerical solutions for the steady-state continuous release: the source is located at $(x_0, y_0) = (20.0\,\text{m}, 26.7\,\text{m})$; (c and d) cross sections at $x = 20.0$ m and $y = 26.7$ m (coinciding with the source) are compared

$$\hat{C}(\alpha, y) = \int_{-\infty}^{\infty} dx\, C(x, y) e^{-i\alpha x}, \quad C = \frac{1}{2\pi} \int_{-\infty}^{\infty} dk\, \hat{C}(\alpha, y) e^{i\alpha x} \tag{53}$$

then Eq. (51) becomes

$$\frac{\partial^2 \hat{C}}{\partial y^2} - \frac{v}{K}\frac{\partial \hat{C}}{\partial y} - \alpha^2 \hat{C} = -\frac{Q_0}{Kh_0}\delta(y), \quad -\infty < y < \infty \tag{54}$$

The boundary conditions [Eq. (52)] become

$$\hat{C} \to 0, \quad y \to \pm\infty \tag{55}$$

The boundary value problem [Eqs. (54) and (55)] can be split into two equivalent problems

$$\frac{\partial^2 \hat{C}_+}{\partial y^2} - \frac{v}{K}\frac{\partial \hat{C}_+}{\partial y} - \alpha^2 \hat{C}_+ = 0, \quad -0+ < y < \infty \tag{56}$$

$$\frac{\partial^2 \hat{C}_-}{\partial y^2} - \frac{v}{K}\frac{\partial \hat{C}_-}{\partial y} - \alpha^2 \hat{C}_- = 0, \quad -\infty < y < 0- \tag{57}$$

with the boundary conditions

$$\hat{C}_\pm \to 0, \quad y \to \pm\infty \tag{58}$$

$$\hat{C}_+ = \hat{C}_-, \quad y = 0 \tag{59}$$

An additional matching condition at $y = 0$ can be obtained by integrating Eq. (54) across the delta function

$$\frac{\partial \hat{C}_+}{\partial y} - \frac{\partial \hat{C}_-}{\partial y} = -\frac{Q_0}{Kk_0}, \quad y = 0 \tag{60}$$

Solutions for Eqs. (56) and (57) can be readily obtained as

$$\hat{C}_+ = A_+ e^{vy/2K} e^{-y\sqrt{(v/2K)^2+\alpha^2}}, \quad y > 0 \tag{61}$$

$$\hat{C}_- = A_- e^{vy/2K} e^{y\sqrt{(v/2K)^2+\alpha^2}}, \quad y < 0 \tag{62}$$

To satisfy Eqs. (59) and (60)

$$A_+ = A_- = \frac{Q_0}{2Kh_0} \frac{1}{\sqrt{\left(\frac{v}{2K}\right)^2 + \alpha^2}} \tag{63}$$

J. Waterway, Port, Coastal, Ocean Eng. 2013.139:437-454.

i.e.,

$$\hat{C} = \frac{Q_0}{2Kh_0} e^{vy/2K} \frac{e^{-|y|\sqrt{(v/2K)^2+\alpha^2}}}{\sqrt{\left(\frac{v}{2K}\right)^2+\alpha^2}}, \quad -\infty < y < \infty \tag{64}$$

Taking the Fourier inverse transform, the concentration solution is found as

$$C(x,y) = \frac{Q_0}{2Kh_0} e^{vy/2K} \frac{1}{2\pi} \int_{-\infty}^{\infty} d\alpha e^{i\alpha x} \frac{e^{-|y|\sqrt{(v/2K)^2+\alpha^2}}}{\sqrt{(v/K)^2+4\alpha^2}}$$

$$= \frac{Q_0}{2Kh_0} e^{vy/2K} \frac{1}{\pi} \int_0^{\infty} \cos(\alpha x) \frac{e^{-|y|\sqrt{(v/2K)^2+\alpha^2}}}{\sqrt{(v/2K)^2+\alpha^2}} d\alpha,$$

$$-\infty < x, y < \infty \tag{65}$$

From Erdelyi et al. (1954, p. 17)

$$\int_0^{\infty} d\alpha \frac{\cos x\alpha \, e^{-\beta\sqrt{\alpha^2+z^2}}}{\sqrt{\alpha^2+z^2}} = K_0\left(z\sqrt{x^2+\beta^2}\right) \tag{66}$$

where K_0 = modified Bessel function of the second kind. Take $\beta \to |y|$, $z = v/2K$

$$C = \frac{Q_0}{2\pi Kh_0} e^{vy/2K} K_0\left(\frac{v}{2K}\sqrt{x^2+y^2}\right) \tag{67}$$

Because of the factor $e^{vy/2K}$, C decays fast on the upstream side ($y < 0$) and slowly on the downstream side ($y > 0$) and spreads out like a plume. If v diminishes with increasing y to a very small value of δv after a finite distance, say $y > Y$, then

$$C \propto \frac{Q_0}{2\pi Kh_0} e^{vy/2K} \ln\left(\frac{\delta v}{2K}\sqrt{x^2+Y^2}\right) \tag{68}$$

which can become large, implying accumulation.

Numerical solutions were carried out for different grid sizes and time steps for a source located at (x_0, y_0), in which case the analytical solution becomes

$$C = \frac{Q_0}{2\pi Kh_0} e^{v(y-y_0)/2K} K_0\left[\frac{v}{2K}\sqrt{(x-x_0)^2+(y-y_0)^2}\right] \tag{69}$$

Fig. 17 depicts the analytical and numerical solutions for a continuous release arbitrarily located at $(x_0, y_0) = (20\,\text{m}, 26.7\,\text{m})$, values of $Q_0 = 1\,\text{m}^3/\text{s}$, $K = 1\,\text{m}^2/\text{s}$, $h_0 = 1\,\text{m}$, $v = 0.1\,\text{m}/\text{s}$, a grid size of $dx = dy = 1\,\text{m}$, and a time step of $dt = 1\,\text{s}$. The domain was defined by $0 < x < 40\,\text{m}$ and $0 < y < 80\,\text{m}$, although images are depicted for $10\,\text{m} < x < 30\,\text{m}$ and $20\,\text{m} < y < 40\,\text{m}$, because close to the boundaries, both solutions differ because of the boundary conditions of the numerical code. A good fit is obtained regardless of the grid size or time increment.

Acknowledgments

This work is supported by National Science Foundation grants to Cornell University. P. Winckler thanks Fulbright and Universidad de Valparaiso for financial assistance in the form of a studentship. C. C. Mei acknowledges the support of the Mary Upson visiting professorship at Cornell University for this collaboration.

References

Clark, D. B., Feddersen, F., and Guza, R. T. (2010). "Cross-shore surfzone tracer dispersion in an alongshore current." *J. Geophys. Res. Oceans*, 115(C10035), 1–18.

Clarke, L. B., Ackerman, D., and Largier, J. (2007). "Dye dispersion in the surf zone: Measurements and simple models." *Cont. Shelf Res.*, 27(5), 650–669.

Erdelyi, A., Magnus, W., and Tricomi, F. G. (1954). *Tables of integral transform. Bateman manuscript project*, Vol. 1, McGraw Hill, New York.

Feddersen, F. (2007). "Breaking wave induced cross-shore tracer dispersion in the surfzone: Model results and scalings." *J. Geophys. Res. Oceans*, 112(C0912), 1–12.

Fischer, H. B., List, J. E., Koh, R. C. Y., Imberber, J., and Brooks, N. H. (1979). *Mixing in inland and coastal waters*, Academic Press, New York.

Harris, T. F. W., Jordaan, J. M., McMurray, W. R., Verwey, C. J., and Anderson, F. P. (1963). "Mixing in the surf zone." *Int. J. Air Water Pollut.*, 7(2), 649–667.

Hunt, J. N., and Johns, B. (1963). "Currents induced by tides and gravity waves." *Tellus*, 15(4), 343–351.

Inman, D. L., Tait, R. J., and Nordstrom, C. E. (1971). "Mixing in the surf zone." *J. Geophys. Res.*, 76(15), 3493–3514.

Longuet-Higgins, M. S. (1964). "Radiation stresses in water waves: A physical discussion, with applications." *Deep-Sea Res.*, 11, 529–562.

Longuet-Higgins, M. S. (1970a). "Longshore currents generated by obliquely incident sea waves, 1." *J. Geophys. Res.*, 75(33), 6778–6789.

Longuet-Higgins, M. S. (1970b). "Longshore currents generated by obliquely incident sea waves, 2." *J. Geophys. Res.*, 75(33), 6790–6801.

Mariani, A. (2004). "A field investigation of dispersion in a surfzone dominated by longshore currents." M. Ocean Eng. thesis, Facolta di Ingegneria, Politecnico di Milano, Milan, Italy, and Coastal Oceanography Group, Univ. of Western Australia, Perth, Australia.

Mei, C. C., and Chian, C. M. (1994). "Dispersion of small suspended particles in wave boundary layers." *J. Phys. Oceanogr.*, 24(12), 2479–2495.

Mei, C. C., Chian, C. M., and Ye, F. (1998). "Transport and resuspension of fine particles in a tidal boundary near a small peninsula." *J. Phys. Oceanogr.*, 28(11), 2313–2331.

Mei, C. C., Fan, S. J., and Jin, K. R. (1997). "Resuspension and transport of fine sediments by waves." *J. Geophys. Res. Oceans*, 102(C7), 15,807–15,821.

Mei, C. C., Stiassnie, M., and Yue, D. K.-P. (2005). *Theory and applications of ocean surface waves. Part 2: Nonlinear aspects*, World Scientific, Singapore.

Munk, W. H. (1949). "The solitary wave theory and its applications to surf problems." *Ann. N.Y. Acad. Sci.*, 51, 376–424.

Pearson, J. M., Guymer, I., West, J. R., and Coates, L. E. (2009). "Solute mixing in the surf zone." *J. Waterway, Port, Coastal Ocean Eng.*, 135(4), 127–134.

Rutherford, J. C. (1994). *River mixing*, Wiley, Chichester, U.K.

Spydell, M., Feddersen, F., and Guza, R. T. (2007). "Observing surfzone dispersion with drifters." *J. Phys. Oceanogr.*, 37(12), 2920–2939.

Spydell, M. S., Feddersen, F., and Guza, R. T. (2009). "Observations of drifter dispersion in the surfzone: The effect of sheared alongshore currents." *J. Geophys. Res.*, 114(C7), 1–12.

Sun, T., and Tao, J.-H. (2003). "Numerical modelling and experimental verification of pollutant transport under waves in the nearshore zone." *Acta Oceanol. Sin.*, 25, 104–112.

Svendsen, I. (2006). *Introduction to nearshore hydrodynamic. Advances series in ocean engineering*, Vol. 24, World Scientific, Singapore.

Takewaka, S., Misaki, S., and Nakamura, T. (2003). "Dye diffusion experiment in a longshore current field." *Coast. Eng. J.*, 45(03), 471–487.

Tao, J.-H., and Han, G. (2002). "Effects of wave motion on pollutant transport in shallow coastal water." *Sci. China, Series E-Technol.*, 45(6), 593–605.